Chemical Geology 328 (2012) 222–243

Contents lists available at SciVerse ScienceDirect

Chemical Geology

journal homepage: www.elsevier.com/locate/chemgeo

Late Early Cretaceous adakitic granitoids and associated magnesian and potassium-rich mafic enclaves and dikes in the Tunchang–Fengmu area, Hainan Province (South China): Partial melting of lower crust and mantle, and magma hybridization

Qiang Wang [a,*], Xian-Hua Li [b], Xiao-Hui Jia [a,e], Derek Wyman [c], Gong-Jian Tang [a], Zheng-Xiang Li [d], Lin Ma [a], Yue-Heng Yang [b], Zi-Qi Jiang [a], Guo-Ning Gou [a]

[a] State Key Laboratory of Isotope Geochemistry, Guangzhou Institute of Geochemistry, Chinese Academy of Sciences, Guangzhou 510640, China
[b] Institute of Geology and Geophysics, Chinese Academy of Sciences, Beijing 100029, China
[c] School of Geosciences, The University of Sydney, NSW 2006, Australia
[d] ARC Centre of Excellence for Core to Crust Fluid Systems (CCFS) and The Institute for Geoscience Research (TIGeR), Department of Applied Geology, Curtin University, Perth, WA 6845, Australia
[e] Wuhan Institute of Geology and Mineral Resources, Wuhan 430223, China

ARTICLE INFO

Article history:
Accepted 26 April 2012
Available online 14 May 2012

Keywords:
Adakites
Shoshonites
Enclaves
Magma mixing
Underplating
South China

ABSTRACT

This paper reports on a rare magmatic suite of adakitic rocks and associated magnesian and potassium-rich magmatic enclaves and dikes, which occur in the Tunchang–Fengmu area, Hainan Island (Southeast China). LA-ICP-MS zircon U–Pb age data show that they were generated in the late Early Cretaceous (~107 Ma). The adakitic rocks, consisting mainly of granodiorites and biotite granites, are high-K calc-alkaline and have low $Mg^{\#}$ values (0.27–0.50). They are geochemically similar to slab-derived adakites, e.g., with high SiO_2, Al_2O_3, Sr, Sr/Y and La/Yb values, low Y and Yb contents, and negligible Eu and positive Sr anomalies. They also have relatively uniform $(^{87}Sr/^{86}Sr)_i$ (0.7086–0.7096), $(^{206}Pb/^{204}Pb)_i$ (18.50–18.61), $(^{207}Pb/^{204}Pb)_i$ (15.56–15.64) and $(^{208}Pb/^{204}Pb)_i$ (38.17–38.44) isotope ratios, with slightly variable $\varepsilon_{Nd}(t)$ (−3.85 to −6.55) and zircon in situ $\varepsilon_{Hf}(t)$ (−4.7 to +1.7) values. The mafic enclaves and dikes display disequilibrium textures (e.g., multiple-zoned clinopyroxene with low-MgO rims in contact with perthite and quartz microcrystals). They are high-K calc-alkaline and shoshonitic, and all but one sample have high $Mg^{\#}$ (0.63–0.72) values. These mafic rocks are characterized by light rare earth element enrichment and heavy rare earth element (REE) depletion, negligible Eu and Sr and positive Pb anomalies, and Nb and Ta depletion. They have slightly more variable initial $^{87}Sr/^{86}Sr$ isotope ratios (0.7064–0.7086), $\varepsilon_{Nd}(t)$ (−5.1 to +0.1) values, and $(^{206}Pb/^{204}Pb)_i$ (18.35–18.50), $(^{207}Pb/^{204}Pb)_i$ (15.45–15.59) and $(^{208}Pb/^{204}Pb)_i$ (38.18–38.70) ratios. One mafic dike sample has zircon in situ $\varepsilon_{Hf}(t)$ values (−4.94 to −2.42) similar to those of adakitic rocks (−4.7 to +1.7) in the area. We suggest that the adakitic rocks were most likely generated by partial melting of newly underplated basaltic lower crust with arc-like geochemical characteristics, and the primitive compositions of the mafic enclaves and dikes likely originated from lithospheric + asthenospheric mantle sources metasomatized by subducted oceanic sediments or a relatively juvenile lithospheric mantle source. Mantle-derived primitive magmas likely underwent mixing at depth with minor crustally-derived felsic magmas before being injected into the adakitic magma chamber. Such injections may have broken up the magma into discrete globules and convective motion distributed the enclaves through the adakitic host. Asthenosphere upwelling due to the roll-back of the subducted Paleo-Pacific plate likely triggered the coeval late Early Cretaceous crust- and mantle-derived magmatism, resulting in the magma hybridization observed on Hainan Island.

1. Introduction

Mafic enclaves often occur in calc-alkaline, alkaline and even peralkaline granitoids, and have attracted wide interests due to their important role in understanding the origin of the host granitoids, deep crustal composition and geodynamic processes (e.g., Didier, 1973; Vernon, 1984; Holden et al., 1987; Eberz et al., 1990; Bonin, 1991; Didier and Barbarin, 1991; Wiebe et al., 1997; Barbarin, 2005; Schonenberger et al., 2006; Yang et al., 2006, 2007; Chen et al., 2009; Shellnutt et al., 2010; Sun et al., 2010). Four main models have been proposed for the formation of the enclaves. First, they may be foreign xenoliths (usually country rocks) incorporated in their solid state during emplacement and/or crystallization of the host magma (e.g.,

* Corresponding author.
E-mail address: wqiang@gig.ac.cn (Q. Wang).

0009-2541/$ – see front matter © 2012 Elsevier B.V. All rights reserved.
doi:10.1016/j.chemgeo.2012.04.029

Vernon, 1983; Bacon, 1986; Xu et al., 2006). Second, they may be recrystallized, refractory and residual phase assemblages, derived from the sources of the granitoid, which did not reach a critical melt fraction during differentiation (e.g., Chappell et al., 1987; Chappell and White, 1991). Third, they may be partly chilled materials or accumulations of early formed genetically related crystals that were trapped in their own residual liquid, usually referred to as "autoliths" (e.g., Tindle and Pearce, 1983; Bonin, 1991; Schonenberger et al., 2006; Shellnutt et al., 2010). Fourth, they may be derived by mixing or mingling between unequal proportions of mafic and felsic magmas, a model supported by both field and petrography observations and by geochemical data from plutonic and volcanic environments (e.g., Holden et al., 1987; Wiebe et al., 1997; Barbarin, 2005; Browne et al., 2006; Yang et al., 2006, 2007; Chen et al., 2009; Kent et al., 2010; Sun et al., 2010). To date, the fourth scenario is more widely applied to the formation of enclaves and even the host granitoids themselves. However, sources of the mafic and felsic magmas involved in the mixing or mingling process remain unclear. For example, the felsic magmas have been attributed to both supracrustal or lower crustal materials (Koyaguchi and Kaneko, 1999; Bonin, 2004; Guo et al., 2007; Streck et al., 2007) and the mafic magmas have been interpreted as originating directly from the mantle or from mafic lower crust (e.g., Silva et al., 2000; Bonin, 2004; Chen et al., 2009; Zhang et al., 2010). These issues are also directly related to uncertainties concerning the source materials and formation mechanisms of the host granitoids.

South China consists of the Yangtze Block in the northwest and the Cathaysia Block in the southeast (Fig. 1a). In recent years, many Jurassic–Cretaceous adakitic intrusive rocks (intermediate-acidic rocks characterized by a depletion of Y and heavy rare earth elements (HREEs), and high Sr/Y and La/Yb ratios) have been documented in the eastern Yangtze Block (e.g., Xu et al., 2002a; Wang et al., 2004a, b, 2006a, b; Huang et al., 2008; Xie et al., 2008; Li et al., 2009; Ling et al., 2009; Liu et al., 2010a; Sun et al., 2011). Only very minor occurrences of adakitic rocks have been reported in the central part of the Cathaysia Block, (e.g., Xiong et al., 2003), however, despite the widespread occurrence of Mesozoic intrusive rocks in the region. In addition, few mafic enclaves have been reported from adakitic plutons in the eastern Yangtze and central Cathaysia Block. During this study, we identified late Early Cretaceous adakitic rocks closely associated with coeval magnesian and potassium-rich mafic magmatic enclaves and dikes in the Tunchang–Fengmu area of the southern Cathaysia Block. We present here field relationships, age data, major and trace element compositional and textural disequilibrium features of some minerals (e.g., clinopyroxene (cpx)), whole-rock chemical and Nd–Sr–Pb isotope data, and in situ zircon Hf isotopic analyses of the mafic enclaves, dikes and host rocks in order to delineate their respective source characteristics and petrogenesis, and their genetic relationships to deep geodynamic processes.

2. Geological background

Mesozoic magmatic rocks are widespread in central and southeastern South China (e.g., Chen and Jahn, 1998; Xu et al., 1999a; Li, 2000; Zhou and Li, 2000; Zhou et al., 2006a; Li and Li, 2007). Hainan Island is generally considered to have been a part of the Cathaysia Block (e.g., Li et al., 2002a, b, 2006a, 2008; Li and Li, 2007) and mainly consists of large-scale Late Permian–Cretaceous granitoids and minor Cretaceous mafic dikes (e.g., Wang et al., 1991; Ge, 2003; Ge et al., 2003; Yun and Xie, 2003; Xie et al., 2005, 2006; Yun et al., 2005; Li et al., 2006a; Li and Li, 2007; Chen et al., 2011; Zhang et al., 2011; Zhao et al., 2012). Exposed metamorphic basement rocks on the island consist of Mesoproterozoic (~1400 Ma) metavolcanic–intrusive–

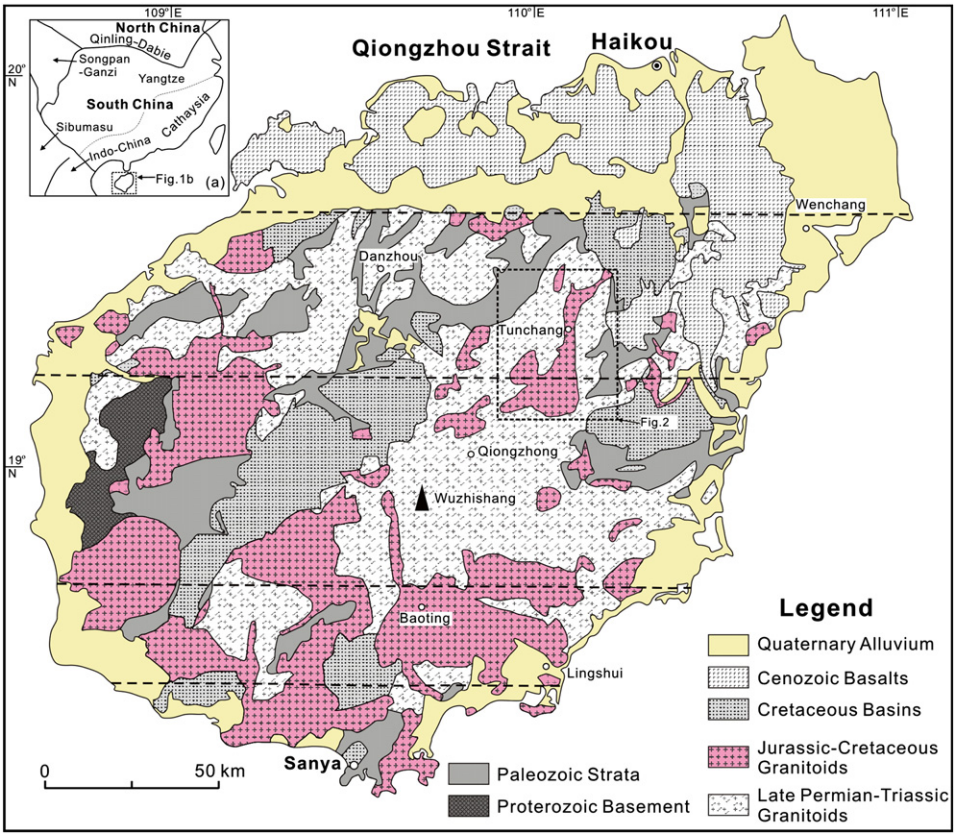

Fig. 1. (a) Distributions of principal continental blocks of Southeast Asia and the Indosinian Fold Belt in South China (After Li et al. (2006a)); (b) A simplified geological map of the Hainan Island. Modified after Wang et al. (1991) and Li et al. (2002a, 2006a).

sedimentary rocks in the Baoban area (Fig. 1b) (e.g., Li et al., 2008). Phanerozoic (Cambrian–Silurian and Carboniferous–Cretaceous) strata (e.g., Wang et al., 1991; Li et al., 2002a, b; Xu et al., 2007, 2008; Zhang et al., 2011), and Cenozoic basalts (e.g., Wang et al., 1991), also crop out on the island.

The Tunchang–Fengmu area is located near central Hainan Island (Fig. 1b). Intrusive rocks in this area consist of gneissic granodiorites and massive intrusive rocks (Fig. 2). The gneissic granodiorites in this study are referred to as "the Huogedun gneissic granodiorites" (Fig. 2). Non-deformed (massive) granodiorites and biotite granites intrude the Huogedun gneissic granodiorite pluton (Fig. 2). The gneissic granodiorites, and the massive granodiorites and biotite granites, were considered to have been generated in the Permian–Triassic and the Cretaceous, respectively (e.g., Wang et al., 1991; Yun and Xie, 2003), but precise age constraints were lacking. The massive Tunchang granodiorite pluton in the Tunchang–Fengmu area is the largest of the Cretaceous massive granodiorite and biotite granite plutons in Hainan, and is distinctly elongate in an approximately NS direction (Fig. 2). Some small biotite granite plutons and mafic and granite dikes occur in, or close to, the pluton, mainly in the Niubiling, Bailing, Gaotongling, Huangzhuling and Machangyuan areas (Fig. 2). The Bailing and Gaotongling biotite granite plutons are associated with Mo mineralization. The Tunchang granodiorite pluton contains sporadic mafic enclaves, which are ellipsoidal, spindle-shaped, or elongate. The biotite granite plutons (e.g., the Niubiling, Gaotongling and Bailing plutons) contain no mafic enclaves. However, mafic dikes intrude both the Tunchang granodiorite and the Gaotongling biotite granite plutons (Fig. 2).

3. Analytical methods

All clinopyroxene mineral analyses and back-scattered-electron imaging were carried out at the State Key Laboratory of Isotope Geochemistry, Guangzhou Institute of Geochemistry, Chinese Academy of Sciences (SKLIG GIG-CAS) with a JEOL JXA-8100 Superprobe. The operating conditions were as the follows: 15 kV accelerating voltage, 20 nA beam current, 1–2 μm beam diameter, 10 s counting time and ZAF correction procedure for data reduction. The analytical procedures were described in detail in Huang et al. (2007).

In situ trace element analysis of clinopyroxene and hornblende was carried out using the laser-ablation (LA)-ICP-MS technique (using an Agilent 7500a ICP-MS system coupled with a GeoLas193 nm ArF-excimer laser sampler) in the SKLIG GIG-CAS. A spot size of 60 μm and a repetition rate of 8 Hz were applied during analysis. Calibration was carried out externally using NIST SRM 610 with Ca as an internal standard to correct for drift if any. Repeated analyses of the USGS rock standards (BHVO-2G and BCR-2G) indicate precision and accuracy both better than 4% for most elements analyzed. The relative standard deviations (RSDs) of rare earth elements (REE), Y, Zr, Hf, Sr, Pb, Sc, Ti and V are better than 6%, and those of Cr, Co, Ni, Ba, Th and U are 3–15%. RSDs of Nb, Ta, Rb and Cs range from 3% to 20%, and from 20% to 50% for low-concentration samples. Analytical details are the same as in Liu et al. (2008, 2010b).

Zircons were separated using conventional heavy liquid and magnetic separation techniques. Zircon grains were handpicked and mounted in an epoxy resin disk, and then polished and coated with gold. Their internal morphology was examined using cathodoluminescence at the

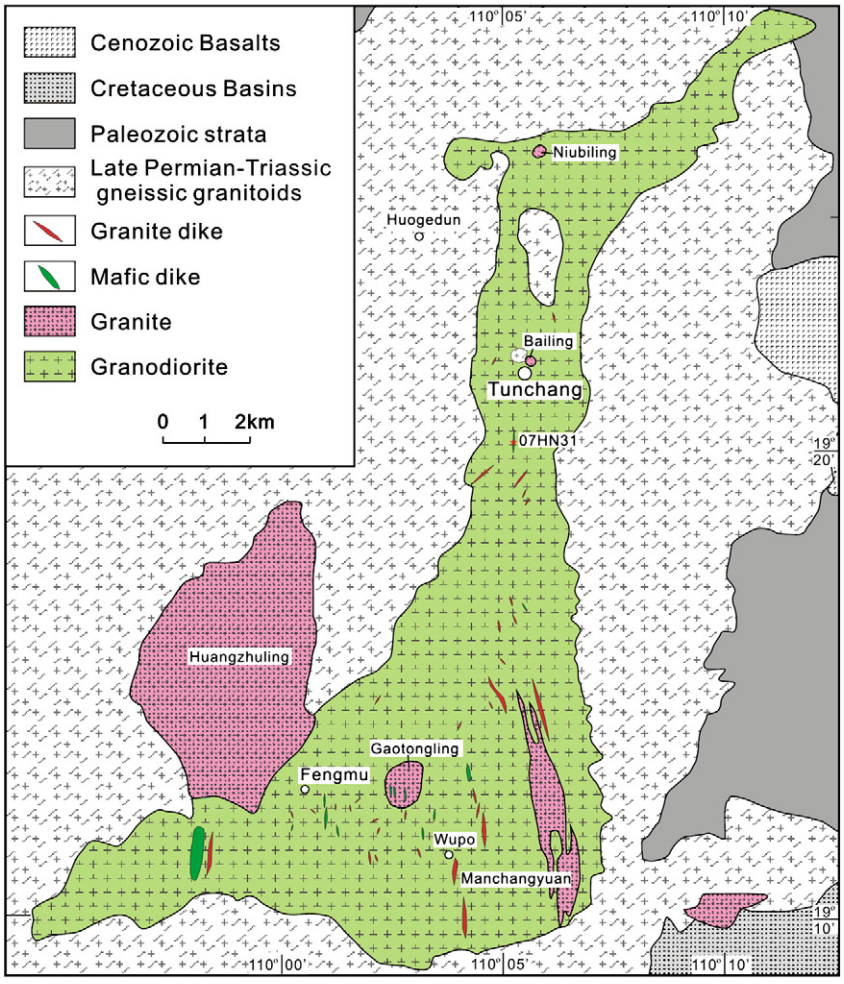

Fig. 2. Geological map of the Tunchang–Fengmu area, Hainan Island.

SKLIG GIG-CAS with a JEOL JXA-8100 Superprobe prior to U–Pb isotopic analysis. The U–Pb isotopic analyses were performed using a LA-ICP-MS at the Institute of Geology and Geophysics, Chinese Academy of Sciences using a Neptune MC-ICP-MS with an ArF excimer laser ablation system. Detailed descriptions of the instrumentation and analytical procedure for the LA-ICP-MS zircon U–Pb technique can be found in Wu et al.

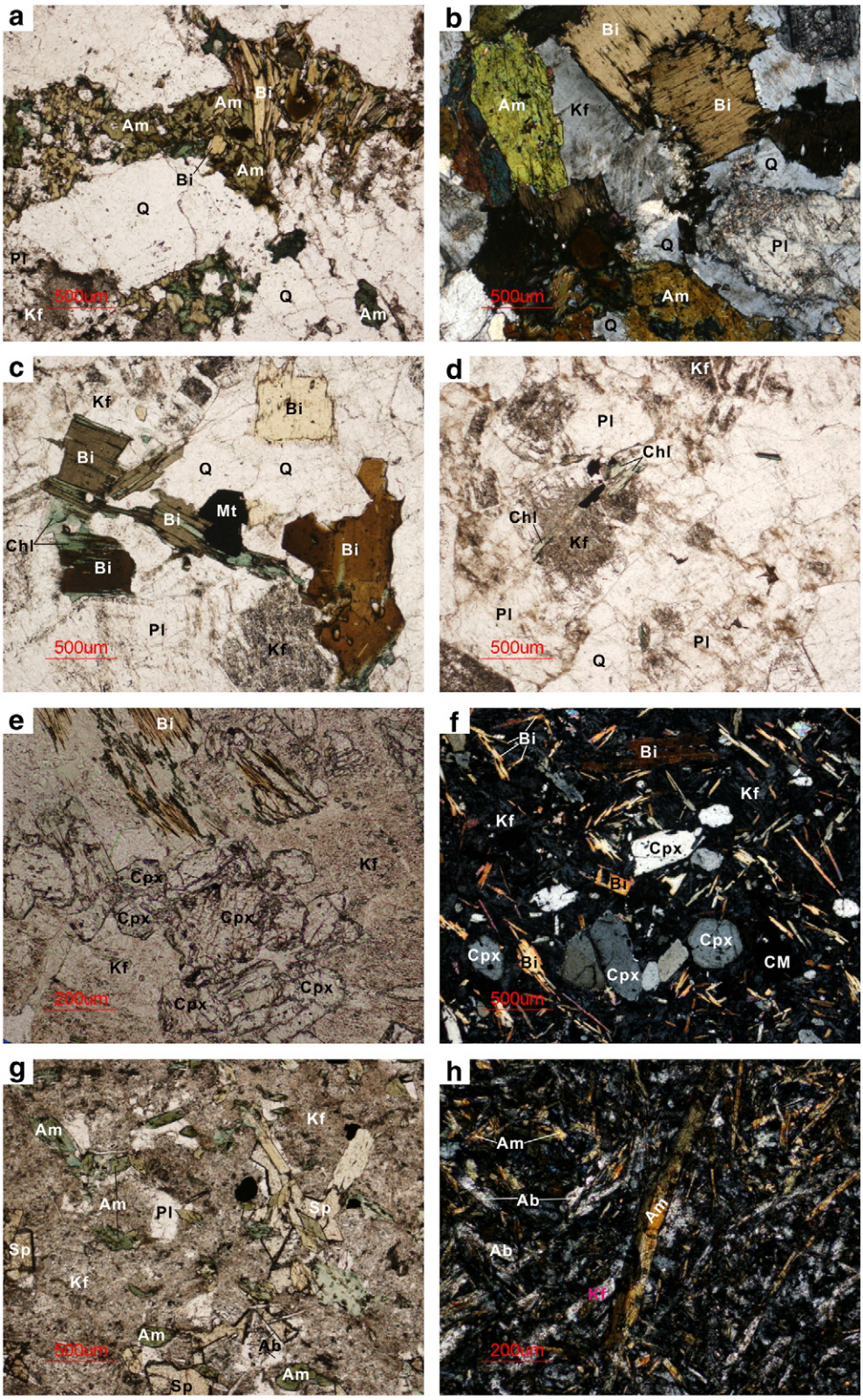

Fig. 3. Photomicrographs of the Tunchang–Fengmu intrusive rocks and associated enclaves and dikes. (a) The gneissic granodiorite (sample 07HN32); (b) the Tunchang granodiorite (sample 07HN08); (c) the Niubiling biotite granites (sample 07HN004); (d) the Gaotongling biotite granite (sample 07HN003); (e) gabbroic enclave (sample 07HN17); (f) diabasic enclaves (sample 07HN21); (g) dioritic enclaves (sample 07HN23); (h) diorite porphyry dike (07HN31). Am—amphibole; Ab—albite; Bi—biotite; Cc—calcite; Chl—chlorite; CM—cryptocrystalline materials; Cpx—clinopyroxene; Kf—feldspar; Mt—magnetite; Pl—plagioclase; Q—quartz; Sp—sphene.

(2006a) and Yang et al. (2006, 2007). The time-resolved spectra were processed off-line using the ICP-MSDATA software (version 3.4; Liu et al. (2008, 2010b)) using zircon 91500 as the external standard. NIST SRM 610 was used as the reference material and ^{29}Si was used as an internal calibrant. Common Pb was corrected using ComPbCorr#3 151 (Andersen, 2002) for those with common $^{206}Pb > 1\%$. Uncertainties in the ages are cited as 1σ, and the weighted mean ages are quoted at the 95% confidence level.

Rock samples were examined under optical microscopy, and unaltered or least-altered samples were selected for geochemical analyses. Major element oxides were determined using the standard X-ray fluorescence (XRF) method (Li et al., 2006b). Trace elements were analyzed using the inductively coupled plasma mass spectrometry (ICP-MS) method on a Perkin-Elmer Sciex ELAN 6000 instrument at SKLIG GIG-CAS. Analytical procedures are the same as those described by Li et al. (2006b). Analytical precision for most elements is better than 3%.

Sr and Nd isotopic analyses were performed on a Micromass Isoprobe multi-collector ICP-MS at the SKLIG GIG-CAS, following analytical procedures described by Li et al. (2006b). Sr and REE were separated using cation columns, and Nd fractions were further separated by HDEHP-coated Kef columns. Measured $^{87}Sr/^{86}Sr$ and $^{143}Nd/^{144}Nd$ ratios were normalized to $^{86}Sr/^{88}Sr = 0.1194$ and $^{146}Nd/^{144}Nd = 0.7219$, respectively. The reported $^{87}Sr/^{86}Sr$ and $^{143}Nd/^{144}Nd$ ratios were respectively adjusted to the NBS SRM 987 standard $^{87}Sr/^{86}Sr = 0.71025$ and the Shin Etsu JNdi-1 standard $^{143}Nd/^{144}Nd = 0.512115$.

For Pb isotopic determination, about 100 mg powder per sample was weighed into the Teflon beaker, then spiked and dissolved in concentrated HF at 180 °C for 7 h. Lead was separated and purified

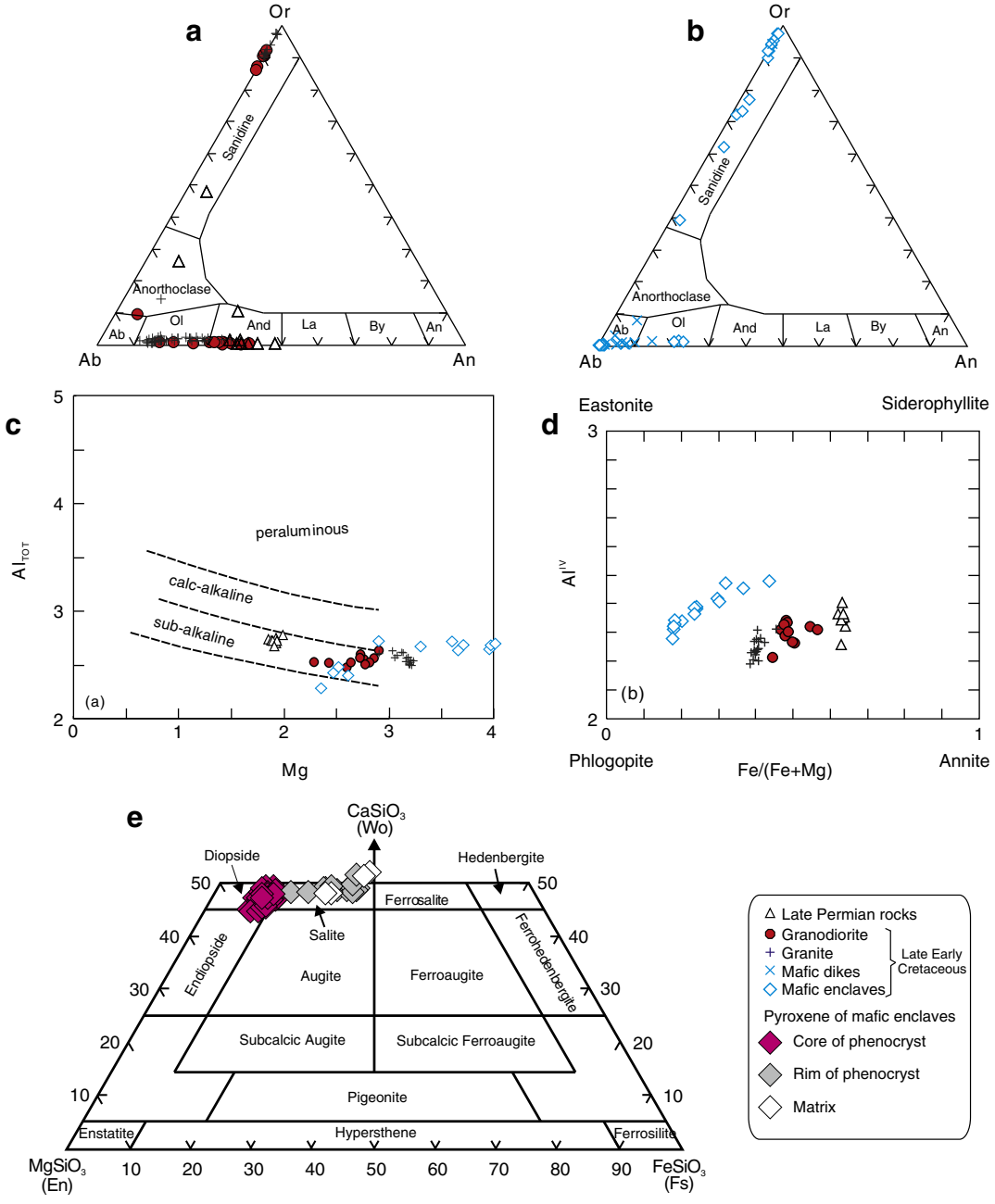

Fig. 4. Chemical characteristics of minerals for the Tunchang–Fengmu intrusive rocks. (a–b) Ab–Or–An diagram for feldspar. Ab—albite; Or—potassium feldspar; An—anorthite; Ol—oligoclase; And—andesine; La—labradorite; By—bytownite. (c) Al_{TOT} vs. Mg diagram for biotite with fields from Nachit et al. (1985). (d) Al^{IV} vs. Fe/(Fe + Mg) diagram for biotite. (e) $CaSiO_3$–$MgSiO_3$–$FeSiO_3$ diagram showing the compositions of pyroxene (Morimoto et al., 1988).

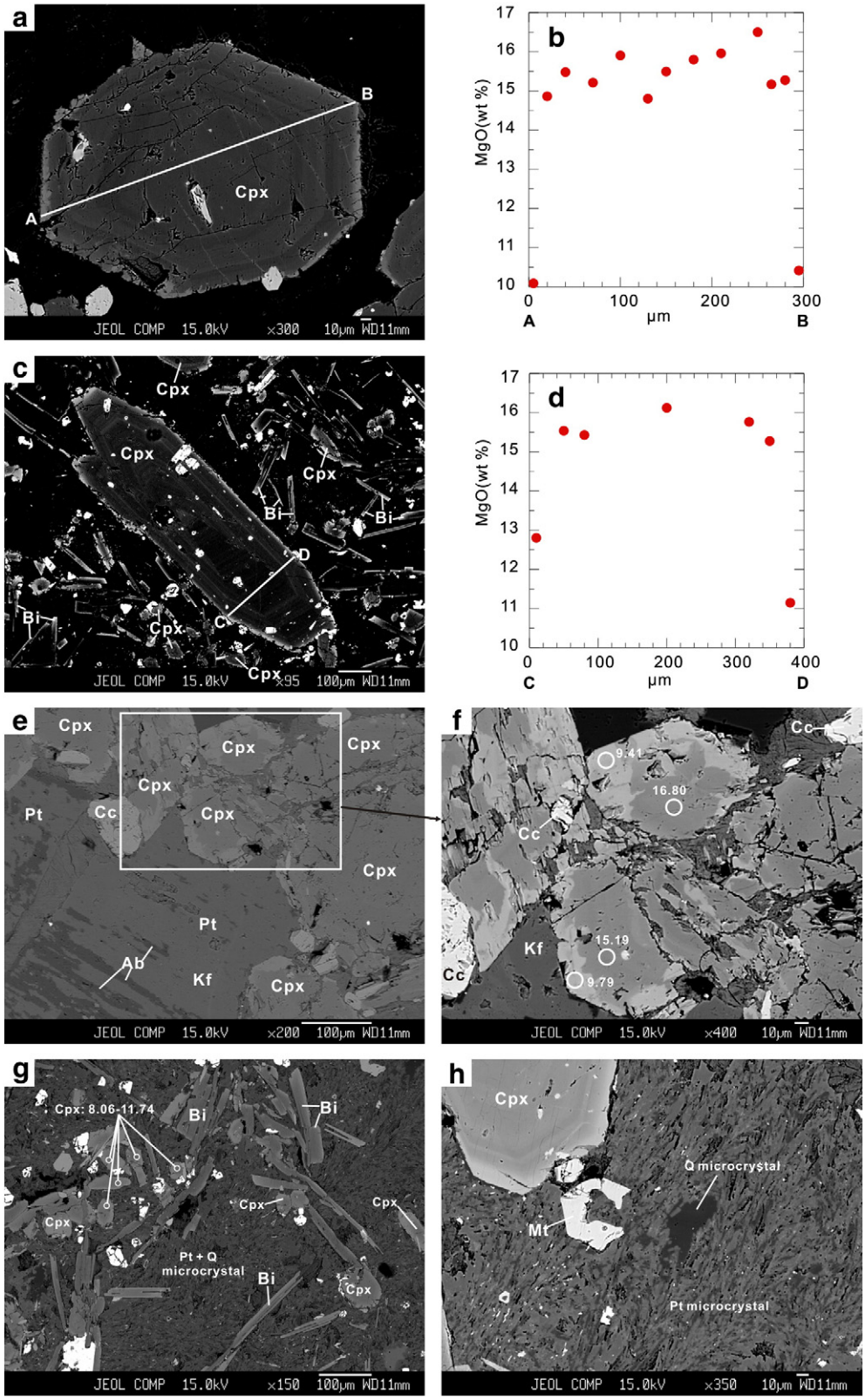

Fig. 5. Disequilibrium features in gabbroic and diabasic enclaves and dikes. (a) Multiple zones in large clinopyroxene crystals (sample 07HN18); (b) MgO contents of multiply zoned clinopyroxene crystals (sample 07HN18); (c) multiply zoned clinopyroxene crystals (sample 07HN21); (d) MgO contents of multiply zoned clinopyroxene granular (sample 07HN21); (e–f) disequilibrium textures between clinopyroxenes and perthites (sample 07HN17); (g) small clinopyroxene crystals (sample 07HN 21); (h) cryptocrystalline materials mainly consisting of perthites + quartz microcrystals in the matrices of diabasic enclaves (sample 07HN21). Ab—albite; Bi—biotite; Cc—calcite; Cpx—clinopyroxene; Kf—feldspar; Mt—magnetite Pt—perthite; Q—quartz. Small circles in Fig. f and g are the analyzed spots for mineral composition, and the numbers (e.g., 9.41) near these circles represent MgO contents (wt.%) of minerals.

by the conventional cation-exchange technique (AG1× 8, 200–400 resin) with diluted HBr as an eluant. Total procedural blanks were less than 50 pg Pb. Isotopic ratios were measured using a VG-354 mass-spectrometer at the GIGCAS following procedures described by Zhu et al. (2001). Repeated analyses of SRM 981 yielded average values of $^{206}Pb/^{204}Pb = 16.900 \pm 4(2\sigma)$, $^{207}Pb/^{204}Pb = 15.498 \pm 4(2\sigma)$ and $^{208}Pb/^{204}Pb = 36.728 \pm 9(2\sigma)$.

In situ zircon Hf isotopic analyses were carried out at the Institute of Geology and Geophysics, Chinese Academy of Sciences using a Neptune MC-ICP-MS with an ArF excimer laser ablation system. During analyses, the spot sizes of 32 and 63 μm and a laser repetition rate of 10 Hz with 100 mJ were used. Details of the technique can be found in Wu et al. (2006a) and Yang et al. (2006, 2007). During analyses, the $^{176}Hf/^{177}Hf$ ratio of standard zircon (91500) was 0.282300 ± 30 (2σ, $n = 23$), similar to the recommended $^{176}Hf/^{177}Hf$ ratio of ~0.282305 (Wu et al., 2006a).

4. Petrography and mineral compositions

Sample names, localities, coordinates, petrography and mineral major element compositions of samples from the Tunchang–Fengmu area are listed in Appendices 1–2. The gneissic granodiorites in the Huogedun area have fine-medium granular texture, and consist of amphibole, biotite, plagioclase, alkaline feldspar, quartz, and accessory minerals (zircon, magnetite and apatite) (Appendix 1). Aggregates of small and xenomorphic amphibole and biotite crystals are commonly distributed around coarser subautomorphic plagioclase, alkaline feldspar and quartz crystals, but are virtually absent within these minerals (Fig. 3a). The alkaline feldspars consist of K-feldspar and anorthoclase; plagioclase has an andesine composition (Fig. 4a; Appendix 2). The biotites plot in the biotite field of sub-alkaline magmatic rocks and exhibit high Fe/(Fe + Mg) ratios (Fig. 4c–d; Appendix 2). Based on the nomenclature of Leake et al. (1997), amphiboles in the gneissic granodiorites are hornblendes (Appendix 2).

The Tunchang granodiorites exhibit a medium granular texture (Fig. 3b), and consist of automorphic–subautomorphic hornblende, biotite, plagioclase, K-feldspar, quartz and minor anorthoclase (Appendices 1–2; Fig. 4a). Their plagioclases consist of andesine and minor oligoclase (Fig. 4a). Their biotites also plot in the biotite field of sub-alkaline magmatic rocks but exhibit lower Fe/(Fe + Mg) ratios than those of the gneissic granodiorites (Fig. 4c–d; Appendix 2). Their accessory minerals include zircon + sphene + ilmenite + magnetite + apatite + epidote + calcite (Appendices 1–2). Ilmenite is commonly in contact with sphene.

The Niubiling and Gaotongling biotite granites have medium to fine-medium granular textures, respectively (Appendix 1). The Niubiling biotite granite mainly consists of automorphic–subautomorphic biotite, plagioclase, K-feldspar, and quartz (Figs. 3c and 4a), and has accessory minerals (zircon + sphene + ilmenite + magnetite + apatite + calcite) similar to those of the Tunchang granodiorites. Their plagioclases consist of oligoclase and minor andesine (Fig. 4a; Appendix 2). Their biotites also plot in the biotite field of sub-alkaline magmatic rocks and exhibit lower Fe/(Fe + Mg) ratios than those of the Huogedun gneissic granodiorites and the Tunchang granodiorites (Fig. 4c–d; Appendix 2). The Gaotongling biotite granite is composed of plagioclase, K-feldspar, quartz and minor biotite (Fig. 3d). Most of the biotite has been altered into chlorite or sericite. Their plagioclases mainly consist of oligoclase (Appendix 2). They contain accessory minerals (zircon + magnetite + apatite + sphene + clinozoisite), but lack ilmenite (Appendix 2).

Gabbroic, diabasic and dioritic mafic enclaves occur in the Tunchang granodiorites (Appendix 1). The gabbroic enclaves exhibit a fine granular texture and consist of clinopyroxene, biotite, K-feldspar or perthite, albite, magnetite, and calcite (Fig. 3e and Appendix 2). Some biotite granules have been altered to chlorite. The diabasic enclaves have porphyritic textures; phenocrysts consist of clinopyroxene, biotite and minor K-feldspar and Quartz (Fig. 3f), and their matrices are composed of small clinopyroxene grains, cryptocrystalline materials and minor titaniferous magnetite and calcite. The dioritic enclaves have medium-fine granular textures (Fig. 3g), and consist of hornblende, plagioclase, K-feldspar, albite, epidote, zircon, magnetite, sphene and calcite (Appendices 1–2). Feldspars in the enclaves are mainly K-feldspar, albite and minor oligoclase (Fig. 4b); no andesine and anorthoclase were found in this study. Their biotites also plot in the biotite field of sub-alkaline magmatic rocks and exhibit the lowest Fe/(Fe + Mg) ratios (Fig. 4c–d; Appendix 2).

Mafic dikes include diabases and diorites, both of which exhibit porphyry textures. The diabase dikes consist of fine-grained plagioclase and albite phenocrysts with lengths of 200–500 μm and matrices, which are composed of smaller clinopyroxene granules (some of which have been altered to chlorite) and cryptocrystalline materials. The diorite porphyries contain amphibole, plagioclase, albite,

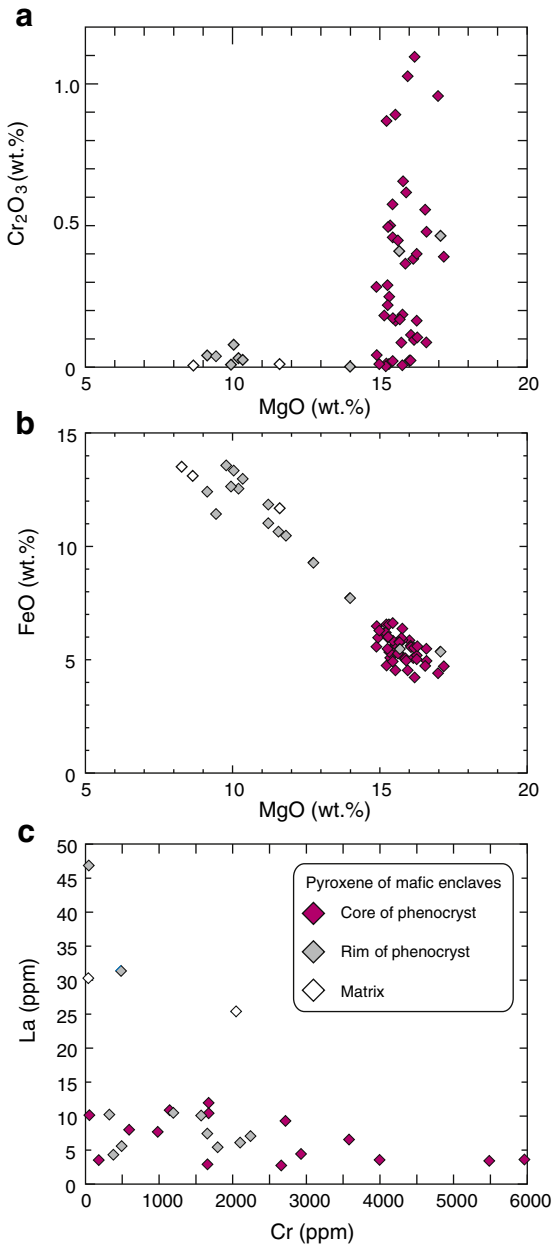

Fig. 6. Major and trace element diagrams for clinopyroxenes from the mafic enclaves in the Tungchang–Fengmu area. (a) MgO versus Cr_2O_3; (b) MgO versus Fe_2O_3; (c) Cr versus La. Major and trace element data for clinopyroxenes are from Appendices 2 to 3.

K-feldspar, zircon and magnetite. Their phenocrysts mainly consist of hornblende, oligoclase, albite and K-feldspar (Figs. 3h and 4b and Appendices 1–2), but no andesine or anorthoclase was found in this study.

There are some disequilibrium textures in the gabbroic and diabasic enclaves and dikes: (1) some larger clinopyroxene phenocrysts exhibit multiple zones (Fig. 5a, c); (2) many clinopyroxene phenocrysts have low MgO (9.02–13.61 wt.%) and Cr_2O_3 (0–1.09 wt.%) and high FeO (4.18–6.61 wt.%) rims and high MgO (14.80–17.14 wt.%) and Cr_2O_3 (0–0.08 wt.%) and low FeO (7.51–13.57 wt.%) cores (Fig. 5a–d; Appendix 2). Low MgO clinopyroxene rims are mainly in contact with perthites (Fig. 5e–f, Appendix 2); (3) some small matrix clinopyroxenes have only low MgO (8.06–11.75 wt.%) and high FeO (10.74–13.17 wt.%) contents (Figs. 5g and 6a–b; Appendix 2); (4) clinopyroxene phenocryst cores exhibit diopside compositions but their rims and small matrix clinopyroxenes mainly have salite compositions (Fig. 4e); (5) all clinopyroxene crystals, including matrix clinopyroxenes and clinopyroxene phenocryst cores and rims, exhibit flat or slightly depleted light rare earth element (LREE) and slightly depleted heavy rare earth element patterns and Nb–Ta depletions (Fig. 7a–b; Appendix 3) but clinopyroxene phenocryst cores generally have more depleted LREE patterns than matrix clinopyroxenes and clinopyroxene phenocryst rims (Fig. 7a; Appendix 3); (6) some clinopyroxene phenocryst cores have high Cr (2659–5963 ppm) and low La (2.75–9.29 ppm), whereas matrix clinopyroxenes and clinopyroxene phenocryst rims have relatively low Cr (<2300 ppm) and variable La (4.33–46.8 ppm) (Fig. 7c); (7) in the matrices of diabasic enclaves, cryptocrystalline materials mainly consist of perthites (Pt) + quartz (Q) microcrystals and are usually in contact with low MgO rims of large or small clinopyroxene crystals (Fig. 5g–h).

5. Geochronology and whole rock geochemistry

5.1. Geochronology

To determine the emplacement ages of the intrusive rocks and dikes in the Tunchang–Fengmu area, five representative samples were chosen for LA-ICP-MS zircon U–Pb dating, one each from the Huogedun gneissic granodiorite, Tunchang granodiorite, Niubiling biotite granite, Gaotongling biotite granite, and one granodiorite porphyry dike to the south of Tunchang town (Fig. 2; Appendix 1). Most zircon crystals fall in the size range of 30 μm (width) × 100 μm (length) to 150 μm × 300 μm. Cathodoluminescence images of zircon grains used for LA-ICP-MS analysis show micro-scale oscillatory zoning (Fig. 8). These zircon grains also exhibit high Th/U ratios (0.14–1.83), suggesting a magmatic origin (Belousova et al., 2002). U–Pb concordia diagrams of analyzed zircons are shown in Fig. 8, and the U–Pb age data are given in Appendix 4.

Twelve zircon analyses from the dominant country rock, gneissic granodiorite (07HN35), give a weighted mean $^{206}Pb/^{238}U$ age of 257 ± 3 Ma (2σ) (mean square weighted deviation (MSWD) = 1.05) (Appendix 4; Fig. 8a). This age is interpreted to be the best estimate of the crystallization age of the Huogedun gneissic granodiorites. The remaining one analysis gives a $^{206}Pb/^{238}U$ age of 516 ± 8 Ma (Fig. 8a), interpreted as the age of inherited zircons.

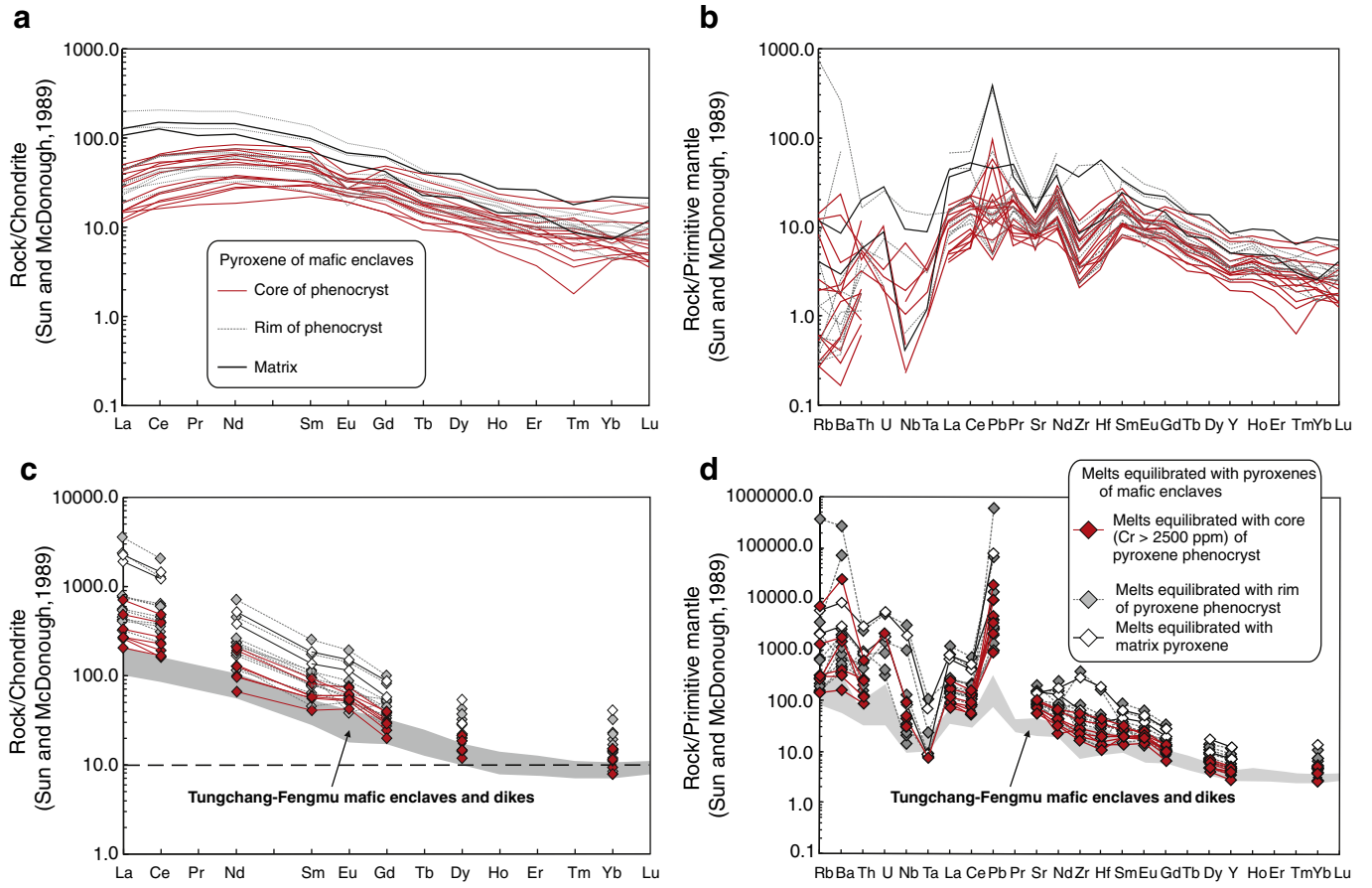

Fig. 7. (a) Chondrite-normalized rare earth element (REE) patterns for clinopyroxenes of mafic enclaves; (b) primitive mantle-normalized trace element patterns for clinopyroxenes of mafic enclaves; (c) chondrite-normalized patterns for calculated REE contents of melts equilibrated with clinopyroxenes in the enclaves; (f) primitive mantle-normalized patterns for calculated trace element contents of melts equilibrated with clinopyroxenes in the enclaves. Chondrite normalizing values and primitive mantle normalizing values are from Sun and McDonough (1989). REE and trace element data are from Appendix 3.

Fifteen analyses of zircons from one sample (07HN19) of the Tunchang granodiorite yield a weighted mean $^{206}Pb/^{238}U$ age of 107.2 ± 1.3 Ma (2σ) (MSWD = 0.71) (Appendix 4; Jia et al., 2010). This age is interpreted to be the best estimate of the crystallization age of the granodiorite. Five other zircon grains have concordant ages of 819 ± 20, 562 ± 9, 252 ± 6, 247 ± 7 and 160 ± 7 Ma, respectively (Appendix 4; Jia et al., 2010). These old (819–160 Ma) zircons were likely inherited from the source rocks or entrained from the wall rocks during the emplacement of the granodiorite.

Thirteen analyses of zircons from one sample (07HN04) of the Niubiling biotite granite result in a weighted mean $^{206}Pb/^{238}U$ age of 107.3 ± 2.4 Ma (2σ) (MSWD = 2.7) (Appendix 4; Jia et al., 2010). This age is interpreted to be the best estimate of the crystallization age of the biotite granite. Three other zircon grains have concordant ages of 244 ± 4, 212 ± 8, 123 ± 4 Ma, respectively (Appendix 4; Jia et al., 2010). These older (244–123 Ma) zircons were likely inherited from the source rocks or entrained from the wall rocks during the granite pluton emplacement.

Twenty analyses of zircons from one sample (07HN11) of the Gaotongling biotite granite give a weighted mean $^{206}Pb/^{238}U$ age of 108.1 ± 1.7 Ma (2σ) (MSWD = 3.5) (Appendix 4; Jia et al., 2010). This age is interpreted to be the best estimate of the crystallization age of the Gaotongling biotite granite.

Thirteen analyses of zircons from one sample (07HN31) of the diorite porphyry dikes yield a weighted mean $^{206}Pb/^{238}U$ age of 107.6 ± 1.5 Ma (2σ) (MSWD = 1.2) (Appendix 4; Fig. 8b). This age is interpreted to be the best estimate of the crystallization age of the dikes in the Tunchang area. The remaining five analyses, giving $^{206}Pb/^{238}U$ ages of 346 ± 5, 168 ± 3 (two analyses), 122 ± 2, and 119 ± 4 Ma, respectively, also plot on or near the U–Pb Concordia curve (Fig. 8b; Appendix 4). These older (346–119 Ma) zircons were likely inherited from the source rocks or entrained from the wall rocks during diorite porphyry emplacement.

5.2. Major and trace elements

Major and trace element data for the intrusive rocks, enclaves and dikes in the Tunchang area are listed in Appendix 5. The Late Early Cretaceous granodiorites and biotite granites, and the Late Permian gneissic granodiorites have clearly lower LOI (loss on ignition) contents (0.47–1.71 wt.%) than the mafic enclaves and dikes (2.14–8.51 wt.%), indicating that the mafic rocks may have undergone alteration and their mobile element (e.g., Rb and Sr) contents may have been modified (e.g., Chung et al., 2001; Wang et al., 2006a). The granodiorites and biotite granites exhibit high SiO_2 (65–74 wt.%) and Al_2O_3 (14.61–16.34 wt.%) and low MgO (0.29–2.05 wt.%) or $Mg^{\#}$ (Mg/(Fe^{total} + Mg)) (0.27–0.50) values, whereas the mafic samples have distinctly lower SiO_2 (48.33–54.63 wt.%), variable Al_2O_3 (11.89–17.66 wt.%) and high MgO (6.0–11.34 wt.%) or $Mg^{\#}$ (0.63–0.72) values, except for one enclave sample with relatively low MgO (4.22 wt.%) and $Mg^{\#}$ (0.47) (Appendix 5).

There is a distinct compositional gap (about 10 wt.% between 56 and 65 wt.%) between the granodiorite–biotite granite and mafic enclave–dike samples (Fig. 9, Appendix 5). On SiO_2 versus $K_2O + Na_2O$ and K_2O diagrams (Fig. 9a, b), the late Early Cretaceous granodiorites and biotite granites, Late Permian gneissic granodiorites and three mafic dike samples plot in the fields of subalkaline and high-K calc-alkaline magmatic rocks, respectively. The mafic enclave samples and the one remaining dike sample plot in the fields of alkaline and shoshonitic magmatic rocks, respectively (Fig. 9a, b). Moreover, enclaves and dike samples with the highest MgO (8.50–11.34 wt.%) and $Mg^{\#}$ (0.66–0.72) values exhibit high K_2O/Na_2O ratios (1.46–2.62) (Appendix 5, Fig. 9c), similar to those of ultrapotassic rocks described by Foley et al. (1987). The most obvious differences between the high-SiO_2 acid and low-SiO_2 samples are that their major oxides (e.g., K_2O and Al_2O_3), trace elements (e.g., Ba) and ratios (e.g., Nb/Ta) exhibit very distinct trends with increasing SiO_2 contents (Fig. 9d–f).

The Late Permian Huogedun granodiorites exhibit rare earth element (REE) and trace element patterns similar to those of the Late Permian–Triassic Wuzishan gneissic granitoids (e.g., Li et al., 2006a) on Hainan Island, such as their enrichment in light REEs (LREEs), depletion in heavy REEs (HREEs), negligible Eu and Sr anomalies, Nb and Ta depletion, and strongly positive Sr and Pb anomalies (Fig. 10a, b). The Huogedun gneissic granodiorite samples do not plot in the field of adakites due to their relatively high Y (19.2–31.5 ppm) and Yb (1.96–2.11 ppm) contents (Fig. 11a). The late Early Cretaceous Tunchang granodiorites and the Niubiling and Gaotongling biotite granites also exhibit enrichment in LREEs, depletion in HREEs, Nb and Ta depletion, and strongly positive Pb anomalies, similar to those of the Hainan Island Late Permian–Triassic granitoids (Fig. 10a, b). However, they have more depleted HREE patterns, negligible Eu anomalies, and positive Sr anomalies (Fig. 10a, b). Moreover, they are characterized by high Sr (396–898 ppm), Sr/Y (54–162) and La/Yb (31–92) values, and low Y (2.95–11.1 ppm) and Yb (0.29–1.19 ppm) contents, and plot in the field of adakites (Fig. 11a). The Niubiling and Gaotongling biotite granites also display more depleted middle REE and HREE (Gd–Lu) patterns than those of the Tunchang granodiorite (Fig. 10a–b).

The mafic enclaves and dikes exhibit similar REE and trace element patterns, e.g., LREE enrichment and HREE depletion, negligible Eu and Sr and positive Pb anomalies, and Nb and Ta depletion (Fig. 10a, b). However, they have relatively high HREE (e.g., Yb =

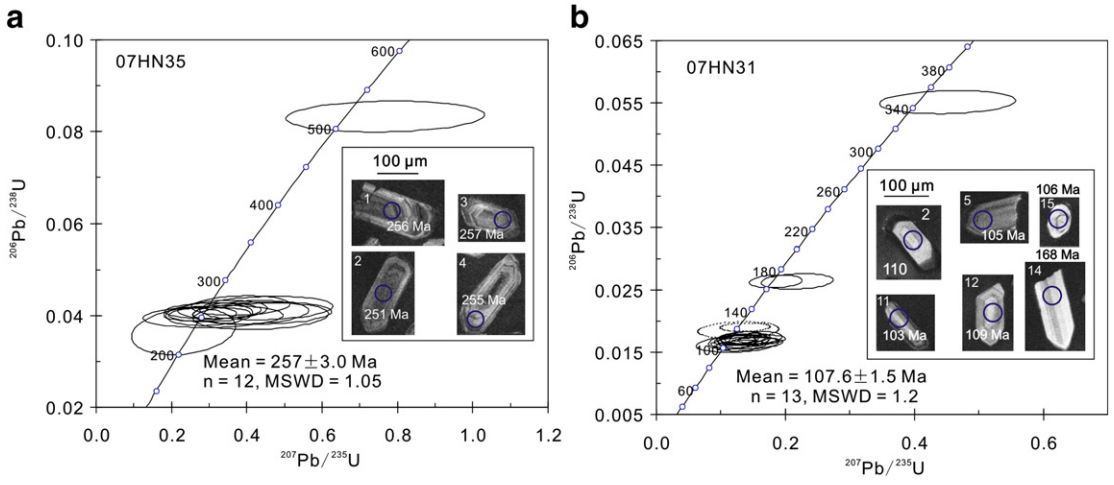

Fig. 8. LA-ICP-MS zircon U–Pb concordia diagram with zircon cathodoluminescence image for the intrusive rocks and dikes in the Tunchang–Fengmu area.

1.21–1.85 ppm) and Y (12.5–20.2 ppm) contents compared to either the Tunchang granodiorite or the Niubiling and Gaotongling biotite granites (Figs. 10c–d and 11a).

5.3. Nd–Sr–Pb–Hf isotope compositions

Nd–Sr–Pb isotope data for the intrusive rocks, enclaves and dikes in the Tunchang–Fengmu area are listed in Appendix 6. All of these rocks have Nd–Sr isotope compositions that differ from those of the Tunchang Paleozoic metamorphic rocks and Baoban Mesoproterozoic basement metamorphic rocks on Hainan Island (Fig. 12a). The Late Permian Huogedun gneissic granodiorites exhibit the lowest $\varepsilon_{Nd}(t)$ values (−10.94) and highest initial $^{87}Sr/^{86}Sr$ isotopic ratios (0.7112–0.7152) among the Late Permian–Early Cretaceous rocks in the Tunchang–Fengmu area, and are comparable to those of Permian–Triassic granitoids on Hainan Island (Appendix 6, Fig. 12a). The Tunchang adakitic granodiorites have initial $^{87}Sr/^{86}Sr$ isotopic ratios (0.7086–0.7091) and $\varepsilon_{Nd}(t)$ values (−3.85 to −5.47), which differ somewhat from those of the Niubiling and Gaotongling adakitic granites (0.7090–0.7096, −5.07 to −6.55) (Appendix 6, Fig. 12a–b). The enclave and dike samples exhibit similar $\varepsilon_{Nd}(t)$ values (−4.61to −5.10) and initial $^{87}Sr/^{86}Sr$ isotopic ratios (0.7080–0.7086) (Appendix 6, Fig. 12a–b). The one exception is enclave sample (07HN018), which has the highest MgO (11.34 wt.%) and $Mg^{\#}$ (0.72) along with a distinctly higher $\varepsilon_{Nd}(t)$ value (0.13) and lower initial $^{87}Sr/^{86}Sr$ isotopic ratio (0.7064).

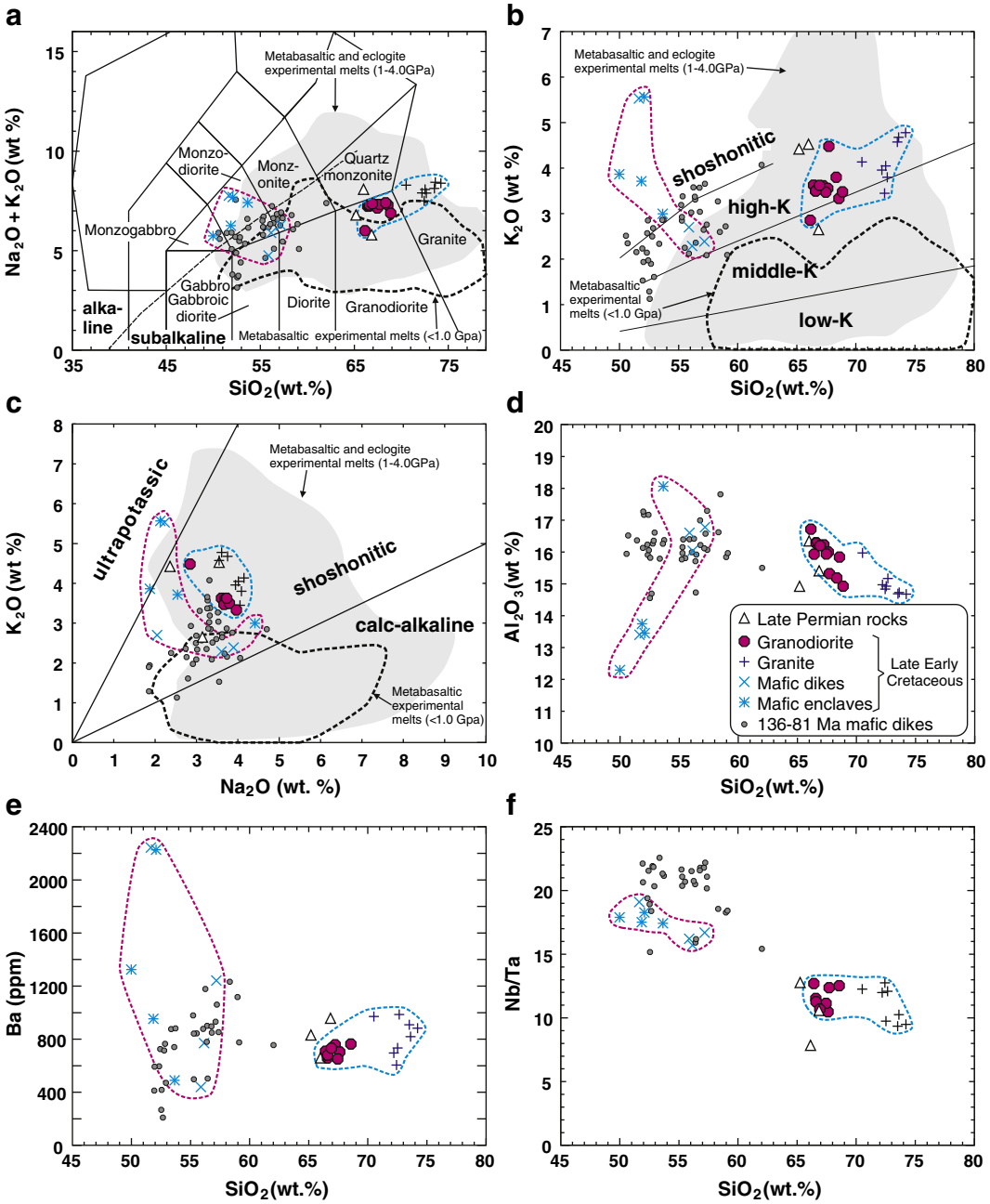

Fig. 9. (a) SiO_2 versus $K_2O + Na_2O$ diagram for intrusive rocks (Middlemost, 1994); (b) SiO_2 versus K_2O (Peccerillo and Taylor, 1976); (c) Na_2O versus K_2O (Peccerillo and Taylor, 1976); (d) SiO_2 versus Al_2O_3 diagram; (e) SiO_2 versus Ba diagram; (f) SiO_2 versus Nb/Ta diagram. The field of metabasaltic and eclogite dehydration experimental melts (1–4.0 GPa) is from the following references (Sen and Dunn, 1994; Rapp and Watson, 1995; Springer and Seck, 1997; Rapp et al., 1999; Skjerlie and Patiño Douce, 2002, and references therein). The field for metabasaltic experimental melts (1–4.0 GPa) is from the following references (Beard and Lofgren, 1991; Robert and Clemene, 1993; Rapp and Watson, 1995). The compositional data for 136–81 Ma mafic dikes in the central Hainan Island are from Ge (2003) and Ge et al. (2003).

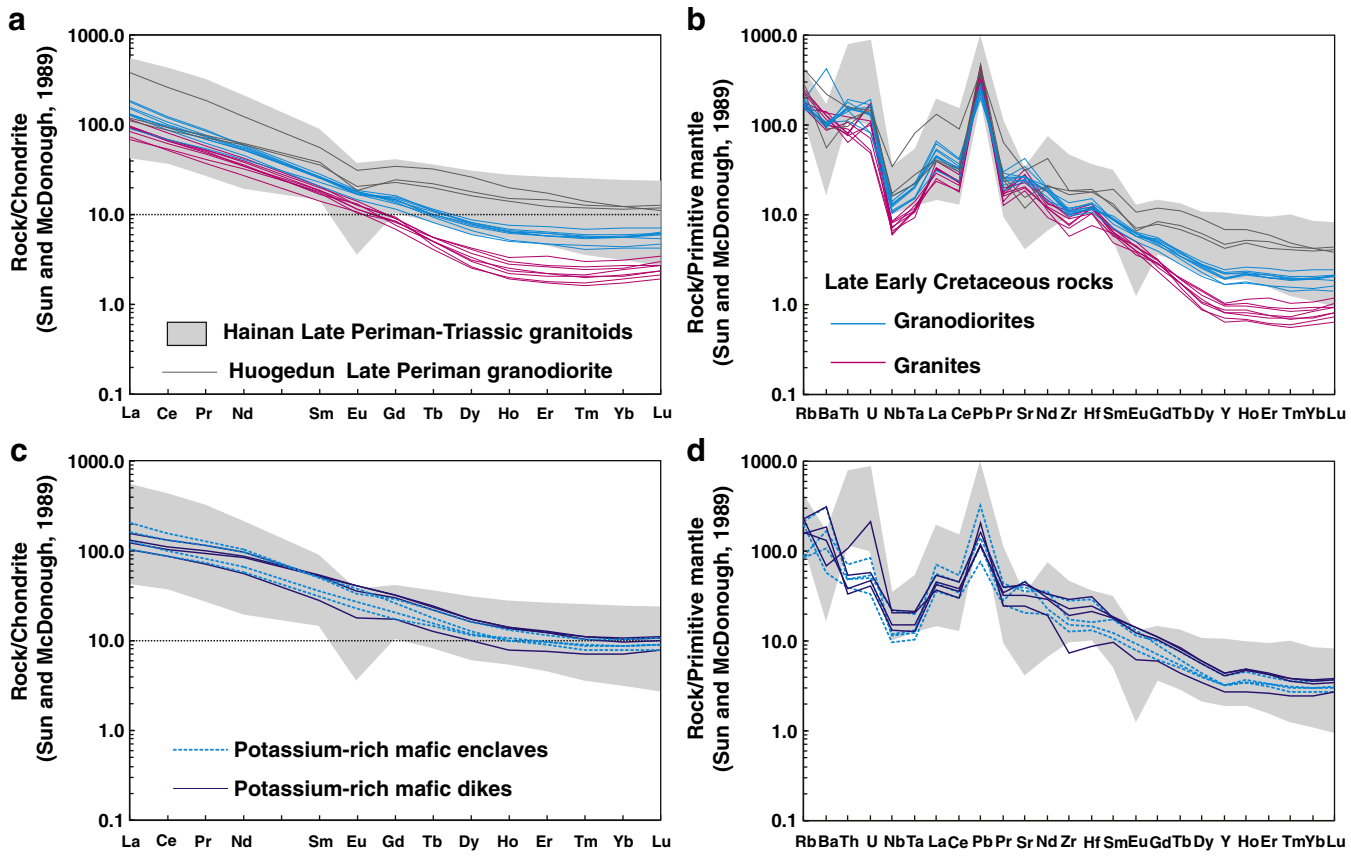

Fig. 10. (a) Chondrite-normalized rare earth element (REE) patterns for the acid intrusive rocks in the Tunchang–Fengmu area; (b) primitive mantle-normalized trace element patterns for the acid intrusive rocks in the Tunchang–Fengmu area; (c) chondrite-normalized REE patterns for the mafic enclaves and dikes rocks in the Tunchang–Fengmu area; (d) primitive mantle-normalized trace element patterns for the mafic enclaves and dikes rocks in the Tunchang–Fengmu area. Chondrite normalizing values and primitive mantle normalizing values are from Sun and McDonough (1989).

Enclave sample 07HN18 also has a Pb isotope composition that is distinct from all other samples in that it has lowest $(^{206}Pb/^{204}Pb)_i$ (18.347), $(^{207}Pb/^{204}Pb)_i$ (15.453) and $(^{208}Pb/^{204}Pb)_i$ (37.700) ratios and plots in the field of Pacific and N-Atlantic MORB (Appendix 6, Fig. 12c–d). All other samples have similar $(^{206}Pb/^{204}Pb)_i$ ratios (18.480–18.667) (Appendix 6, Fig. 12c–d). However, they have slightly different $(^{207}Pb/^{204}Pb)_i$ and $(^{208}Pb/^{204}Pb)_i$ ratios: 15.624 and 38.177–38.288 for the Huogedun gneissic granodiorites, 15.594–15.640 and 38.331–38.441 for the Tunchang adakitic granodiorites, 15.559–15.638 and 38.168–38.342 for the Niubiling and Gaotongling adakitic granites, and 15.569–15.590 and 38.064–38.183 for other mafic enclave and dike samples, respectively (Appendix 6, Fig. 12a–c).

In situ zircon Hf isotope data for the intrusive rocks and dikes in the Tunchang–Fengmu area are listed in Appendix 7. The ~107 Ma zircons from the Tunchang (07HN19) adakitic granodiorite and the Niubiling (07HN04) and Gaotongling (07HN11) adakitic granite samples have similar Hf isotope compositions with $\varepsilon_{Hf}(t)$ values ranging from −4.7 to 1.72 (weighted average: -1.6 ± 0.4) and T_{DM2} values ranging from 1.12 to 1.54 Ga (average 1.34 Ga) (Fig. 13a–c, Appendix 7). The old (119–819 Ma) zircons from these adakitic

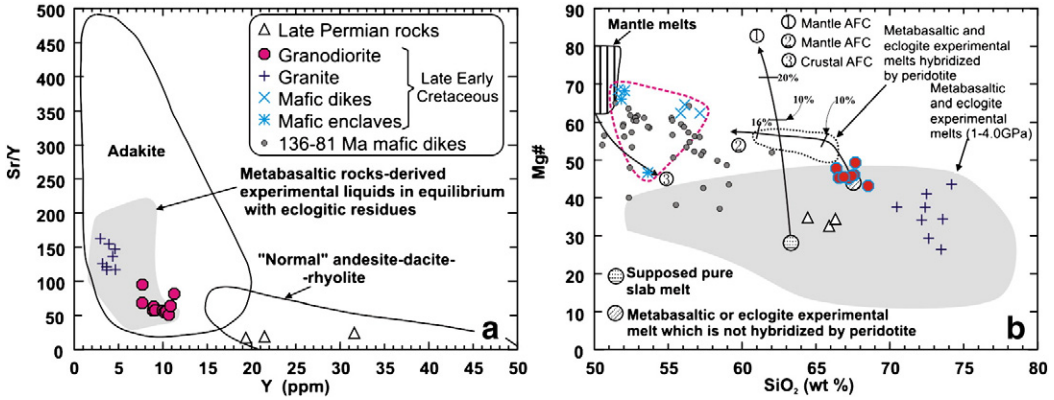

Fig. 11. (a) Sr/Y versus Y diagrams (after Defant et al. (2002)); (b) SiO_2 versus $Mg^{\#}$. The field of metabasaltic and eclogite experimental melts (1–4.0 GPa) is from the following references (Sen and Dunn, 1994; Rapp and Watson, 1995; Springer and Seck, 1997; Rapp et al., 1999; Skjerlie and Patiño Douce, 2002, and references therein).

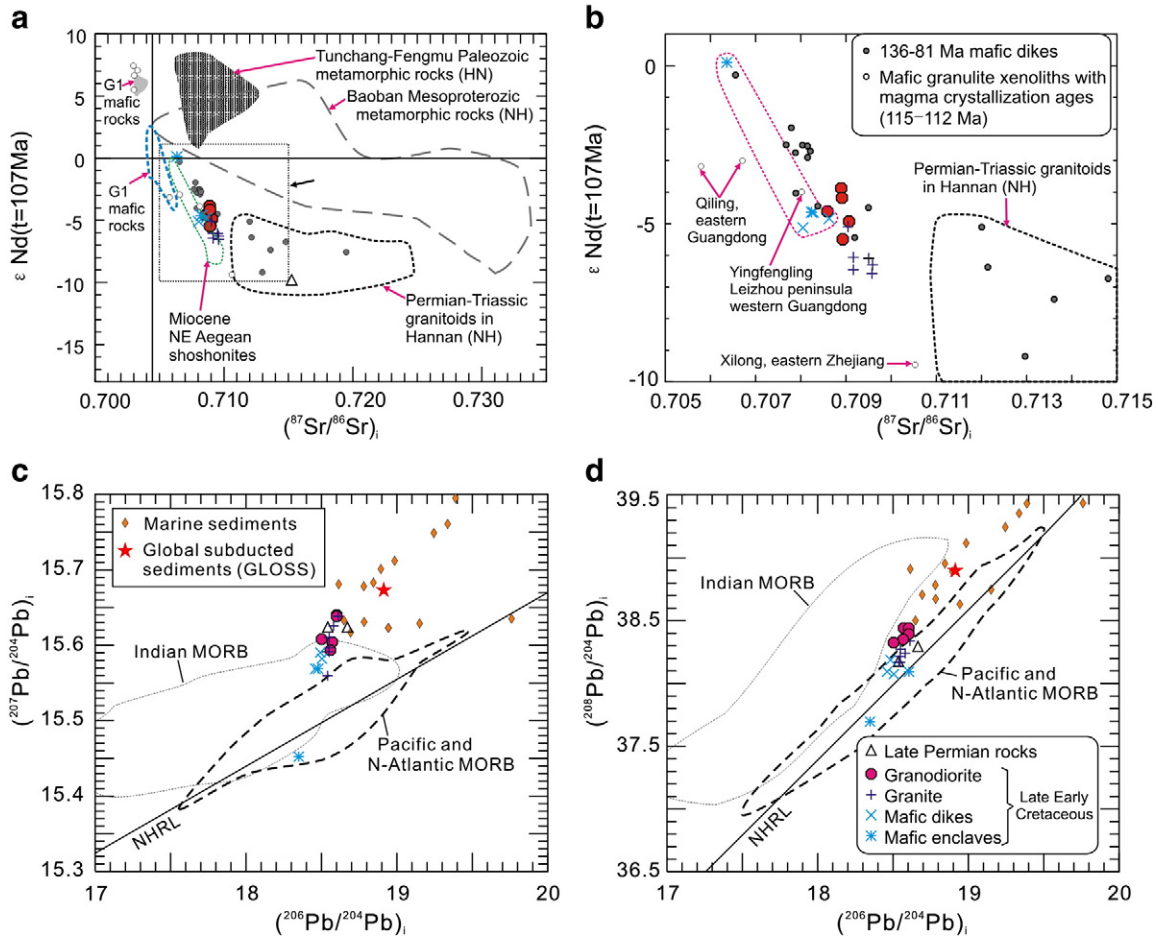

Fig. 12. (a–b) Nd–Sr isotope composition and (c–d) Pb isotope composition diagrams for the intrusive rocks in the Tunchang–Fengmu area. The data for the Baoban Mesoproterozoic metamorphic rocks in the Hainan Island are from (Xu et al., 2000; Li et al., 2008, and references therein). The data for the Paleozoic metamorphic rocks in the Tunchang–Fengmu area are from Xu et al. (2007, 2008). The data for Cretaceous (136–81 Ma) mafic dikes in the central Hainan Island are from Ge (2003) and Ge et al. (2003). The data for Permian–Triassic granitoids in the Hannan Island are from Yun et al. (2005) and Li et al. (2006a). The data for 115–112 Ma lower crustal mafic granulite xenoliths from Cenozoic basalts in the coast of southeast China are after Xu et al. (1996, 1999b) and Yu et al. (2003). The data for Middle Jurassic (~175–170 Ma) mafic rocks derived from an asthenospheric mantle source (Group 1) and Jurassic–Cretaceous (175–145 Ma) mafic rocks derived from enriched subcontinental lithospheric and asthenospheric mantle source (Group 2) in central South China are after from Wang et al. (2008c). The Pb isotope fields for Indian MORB and Pacific and N-Atlantic MORB after Xu et al. (2002b). The data for marine sediments are from Plank and Langmuir (1998). The field for Miocene NE Aegean shoshonites is after Pe-Piper et al. (2009).

rocks have variable $\varepsilon_{Hf}(t)$ (−26.3–0.74) and T_{DM2} (1.2–2.9 Ga) values (Appendix 7). The ~107 Ma zircons from the mafic dike sample (07HN031) have $\varepsilon_{Hf}(t)$ values ranging from −4.94 to −2.42 (weighted average -3.7 ± 0.4) and T_{DM2} values range from 1.38 to 1.55 Ga (average: 1.47 Ga) (Fig. 13d, Appendix 7), which are similar to those of the adakitic rocks (Fig. 13a–c). They also have older (119–346 Ma) zircons with variable $\varepsilon_{Hf}(t)$ (−15.18 to −0.84) and T_{DM2} (1.3–2.2) values (Appendix 7). The ~257 Ma zircons from the Huogedun granodiorite sample (07HN35) have $\varepsilon_{Hf}(t)$ (−8.65 to −2.30, weighted average: -6.1 ± 1.0) and T_{DM2} (1.32–1.72 Ga, average 1.55 Ga) values (Fig. 13e), which are distinct from those of the ~107 Ma zircons from the adakitic rocks and dike sample (Fig. 13a–d). This sample also contains one old (516 Ma) zircon with $\varepsilon_{Hf}(t)$ (−11.92) and T_{DM2} (1.93 Ma) values. In addition, the elder (819–119 Ma) zircon crystals from the adakitic rock and dike samples and one old (516 Ma) zircon from the ~257 Ma Huogedun granodiorite sample may be subdivided into three groups based on their ages and Hf isotope compositions: 212–819 Ma zircons with low and negative $\varepsilon_{Hf}(t)$ values (−26.39 to −5.44) (Fig. 13f); 160–168 Ma zircons with a narrow range of $\varepsilon_{Hf}(t)$ values (−2.96–0.74) except for one granular zircon with a negative $\varepsilon_{Hf}(t)$ value (−12.72) (Fig. 13g); and 119–127 Ma zircons with $\varepsilon_{Hf}(t)$ values (−3.91 to −0.84, weighted average -2.0 ± 1.5) (Fig. 13h).

6. Discussion

6.1. Petrogenesis

6.1.1. Adakitic rocks via partial melting of newly underplated lower crust

Adakitic rocks may be generated by several processes, including (a) melting of subducted young and hot oceanic crust (Mechanism A; Defant and Drummond, 1990; Kay et al., 1993; Stern and Kilian, 1996; Martin et al., 2005; Zhou et al., 2006b; Wang et al., 2007a, 2008a; Tang et al., 2010); (b) partial melting of delaminated lower crust (Mechanism B; Kay and Kay, 1993; Rudnick, 1995; Xu et al., 2002a; Gao et al., 2004; Wang et al., 2006a, b, 2007b; Huang et al., 2008; Zhang et al., 2010); (c) partial melting of subducting continental crust (Mechanism C; Wang et al., 2008b); (d) assimilation and fractional crystallization (AFC) or fractional crystallization (FC) from parental basaltic magmas (Mechanism D; Castillo et al., 1999; Macpherson et al., 2006; Richards and Kerrich, 2007; Li et al., 2009); (e) magma mixing between felsic and basaltic magmas (Mechanism E; Guo et al., 2007; Streck et al., 2007); (f) partial melting of thickened basaltic lower crust (Mechanism F; Atherton and Petford, 1993; Rudnick, 1995; Petford and Atherton, 1996; Chung et al., 2003; Wang et al., 2005a, 2007c). Based on petrologic and geochemical observations, we suggest that the first five models are

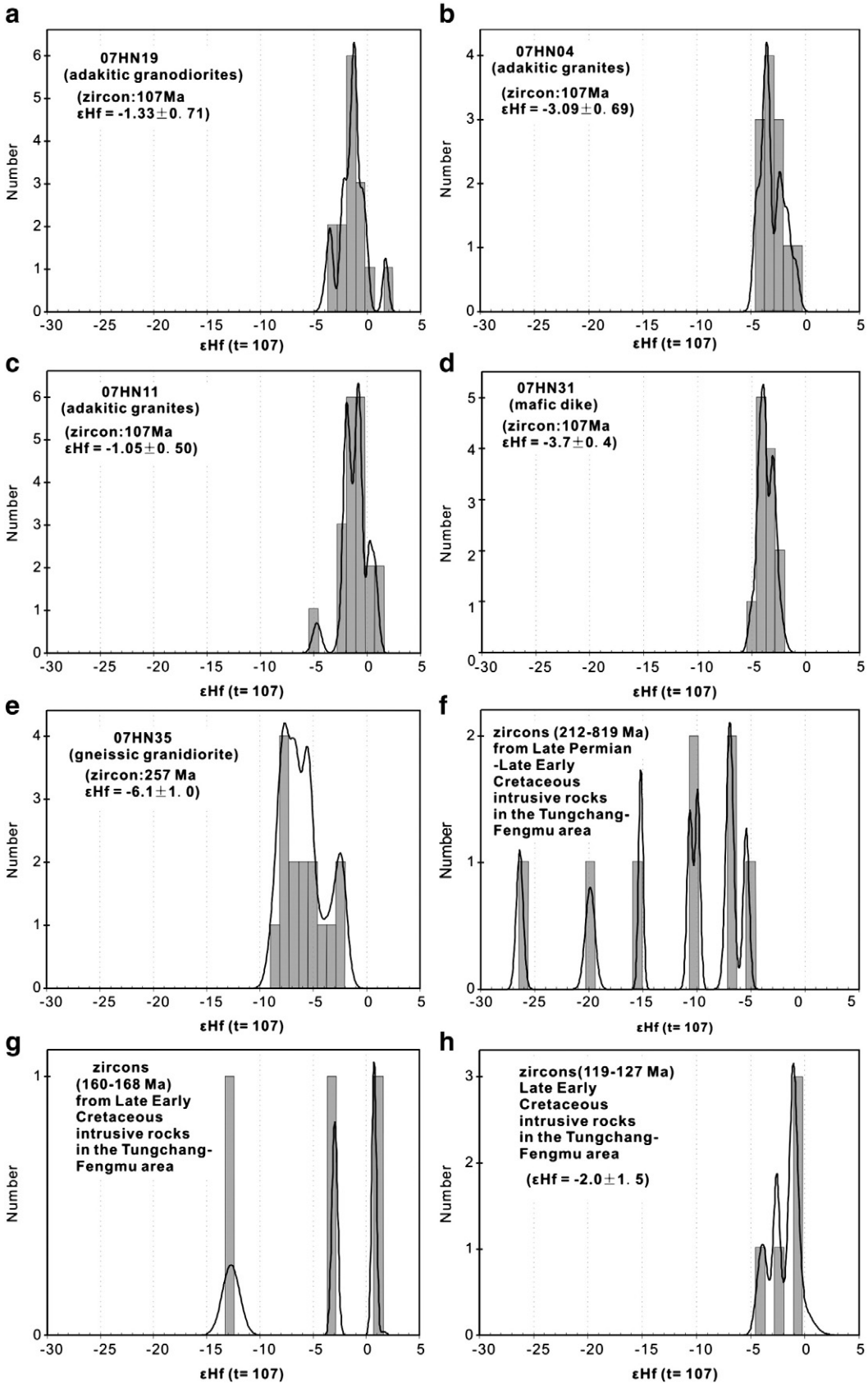

Fig. 13. Histogram of initial Hf isotope ratios for the intrusive rocks and dikes in the Tunchang–Fengmu area.

unlikely explanations for the petrogenesis of the Tunchang–Fengmu adakitic intrusive rocks, whereas the last model seems more plausible.

6.1.1.1. Mechanisms A–E. In general, adakitic rocks generated by mechanisms A–C have high $Mg^{\#}$ values (>0.50) or are similar to high-Mg andesites because their MgO or $Mg^{\#}$ values are increased by the

interaction between magmas derived from subducted oceanic crust, subducted continental crust or delaminated lower crust and mantle peridotites during magma ascent (Fig. 11b) (e.g., Kay et al., 1993; Stern and Kilian, 1996; Rapp et al., 1999; Xu et al., 2002a; Gao et al., 2004; Wang et al., 2006a, b, 2007a, b, 2008a, b; Huang et al., 2008; Tang et al., 2010; Zhang et al., 2010). However, the Tunchang–Fengmu adakitic granodiorites and granites have low MgO (0.29–2.05 wt.%) or $Mg^{\#}$ (0.27–0.50) values (Appendix 5), indicating that interaction between felsic magmas and mantle peridotites was unlikely (Fig. 11b).

Magmatic rocks generated by FC processes generally exhibit continuous compositional trends from basaltic rocks derived from mantle to felsic rocks derived from residual magmas (e.g., Castillo et al., 1999; Macpherson et al., 2006; Li et al., 2009). However, the Tunchang–Fengmu adakitic granodiorites and granites exhibit different compositional trends compared to those of the mafic enclaves and dikes in the area and other Cretaceous (136–81 Ma) mafic dikes on Hainan Island (Fig. 9) (Ge, 2003; Ge et al., 2003). Moreover, they have a compositional trend that is inconsistent with fractional crystallization trends of plagioclase, garnet and amphibole (Fig. 14). In addition, petrographic observations and mineral analyses demonstrate that the mafic enclaves and dikes in the Tungchang–Fengmu area contain K-feldspar, albite, clinopyroxene, biotite, minor oligoclase, hornblende and quartz, but no andesine, anorthoclase or garnet (Appendix 1; Fig. 4a). Given that albite and clinopyroxene are absent in the adakitic biotite granites and granodiorites (Appendix 1; Fig. 4a), it might be suggested that fractional crystallization of these minerals from mafic magmas with compositions similar to the mafic enclaves and dikes could produce the adakitic granites and granodiorites of the Tunchang–Fengmu area. The flat or slightly LREE-depleted patterns for mafic enclave clinopyroxenes (Fig. 7a) indicate, however, that any magmas resulting from the fractional crystallization of clinopyroxene from mafic magmas should exhibit higher LREE contents than their parent magmas. In contrast, the adakitic granites and granodiorites have LREE contents that are similar to or lower than mafic enclaves and dikes in the Tunchang–Fengmu area (Fig. 10a and c), thereby ruling out the clinopyroxene fractional crystallization model. Given that the fractional crystallization of albite from mafic magmas will cause an increase of K_2O in residual magmas, the fact that Tunchang–Fengmu adakitic rocks exhibit much lower K_2O contents than some mafic enclave and dike samples (Fig. 9b) indicates that they were not generated by fractional crystallization of albite.

Crustal assimilation or magma mixing mechanisms usually require a crustally-derived end-member magma, or at least a crustal end-member component (Castillo et al., 1999; Li et al., 2009; Guo et al., 2007; Streck et al., 2007). If the Tunchang–Fengmu adakitic granodiorites and granites were generated by crustal assimilation, then a crustal end-member component is needed with low Y and εNd(t) values and high Sr/Y and initial $^{87}Sr/^{86}Sr$ ratios (Fig. 15a–d). However, no such end-member is present among the Mesoproterozoic–Triassic metamorphic and magmatic rocks on Hainan Island (Fig. 15a–d). Although it initially appears plausible that the Tunchang adakitic granodiorites were generated by mixing between mantle-derived magmas similar to mafic enclaves and dikes and crust-derived granitic magmas similar to the Niubiling and Gaotongling adakitic granites (Fig. 15a–d), several factors indicate that this was not the case. First, the adakitic granodiorites dominate among late Early Cretaceous magmatic rocks in the Tunchang–Fengmu area while the volumes of the contemporary adakitic granites and mafic rocks are much smaller, and few intermediate diorites exist (Figs. 2 and 9). Moreover, the Tunchang adakitic

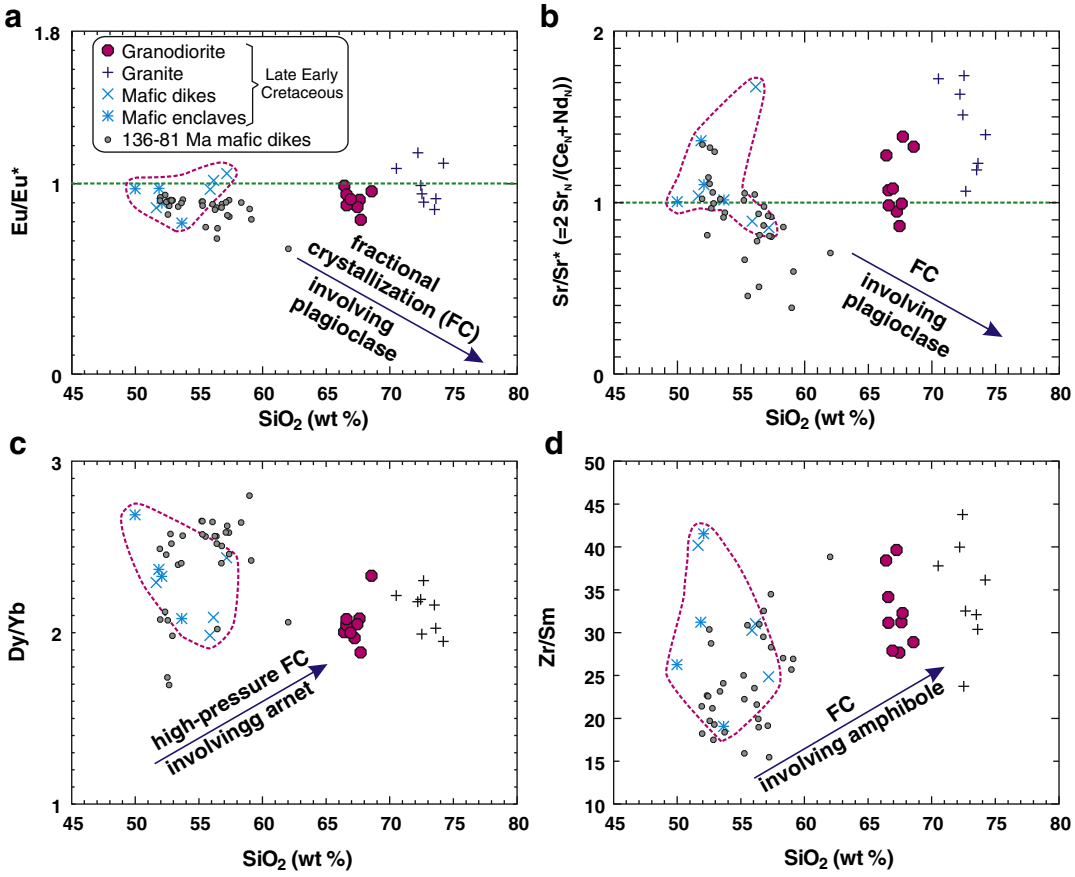

Fig. 14. (a) SiO_2 versus Eu/Eu^*; (b) SiO_2 versus Sr/Sr^*; (c) SiO_2 versus Dy/Yb; (d) SiO_2 versus Zr/Sm. Due to the incompatibility of Zr and compatibility of Sm in hornblende (Drummond et al., 1996), the fractional crystallization will cause the increasing of Zr/Sm ratios in residual magmas. The data for Cretaceous (136–81 Ma) mafic dikes in the central Hainan Island are from Ge (2003) and Ge et al. (2003).

granodiorites are mainly acidic (SiO_2 = 65–68 wt.%) and low in MgO or $Mg^{\#}$ values (Appendix 5 and Figs. 11b and 15e–f), and there is a distinct compositional gap (in SiO_2 and $Mg^{\#}$) between them and the mafic enclaves and dikes in the area (Figs. 9, 11b and 15e–f). The adakitic granodiorites and biotite granites also exhibit compositional trends that are inconsistent with crustal assimilation and magma mixing on εNd(t) vs. $Mg^{\#}$ and SiO_2 diagrams. The granite sample with the highest εNd(t) and $Mg^{\#}$ values (Fig. 15e) exhibits the highest SiO_2 contents (Fig. 15f). Moreover, εNd(t) values for the granites slightly increase with increasing SiO_2 contents (Fig. 15f). This indicates that magma mixing did not play an important role in their formation because magma mixing usually forms intermediate and high Mg (e.g., adakitic high-Mg andesites) rather than acidic adakitic rocks (e.g., Guo et al., 2007; Streck et al., 2007). In addition, the Tunchang adakitic granodiorites have εHf (t), $^{208}Pb/^{204}Pb$ and $^{207}Pb/^{204}Pb$ values close to or slightly higher than those of the mafic dikes, but similar to those of the adakitic granites (Figs. 13a–d and 12c–d), strongly indicating that direct contributions of mantle-derived magmas were very limited in their formation. Therefore, we suggest that the Tungchang–Fengmu adakitic granodiorites and granites could not have been generated by Mechanism D either.

6.1.1.2. Mechanism F. The Tungchang–Fengmu adakitic granodiorites and granites were most probably generated by partial melting of a thickened eclogitic lower crust, based on the following geochemical evidence. First, the adakitic granodiorites and granites have high Sr/Y and low Y values, similar to those of experimental melts of metabasaltic rocks in equilibrium with eclogitic residues (Fig. 11b). Second, they have low $Mg^{\#}$ values similar to those of experimental

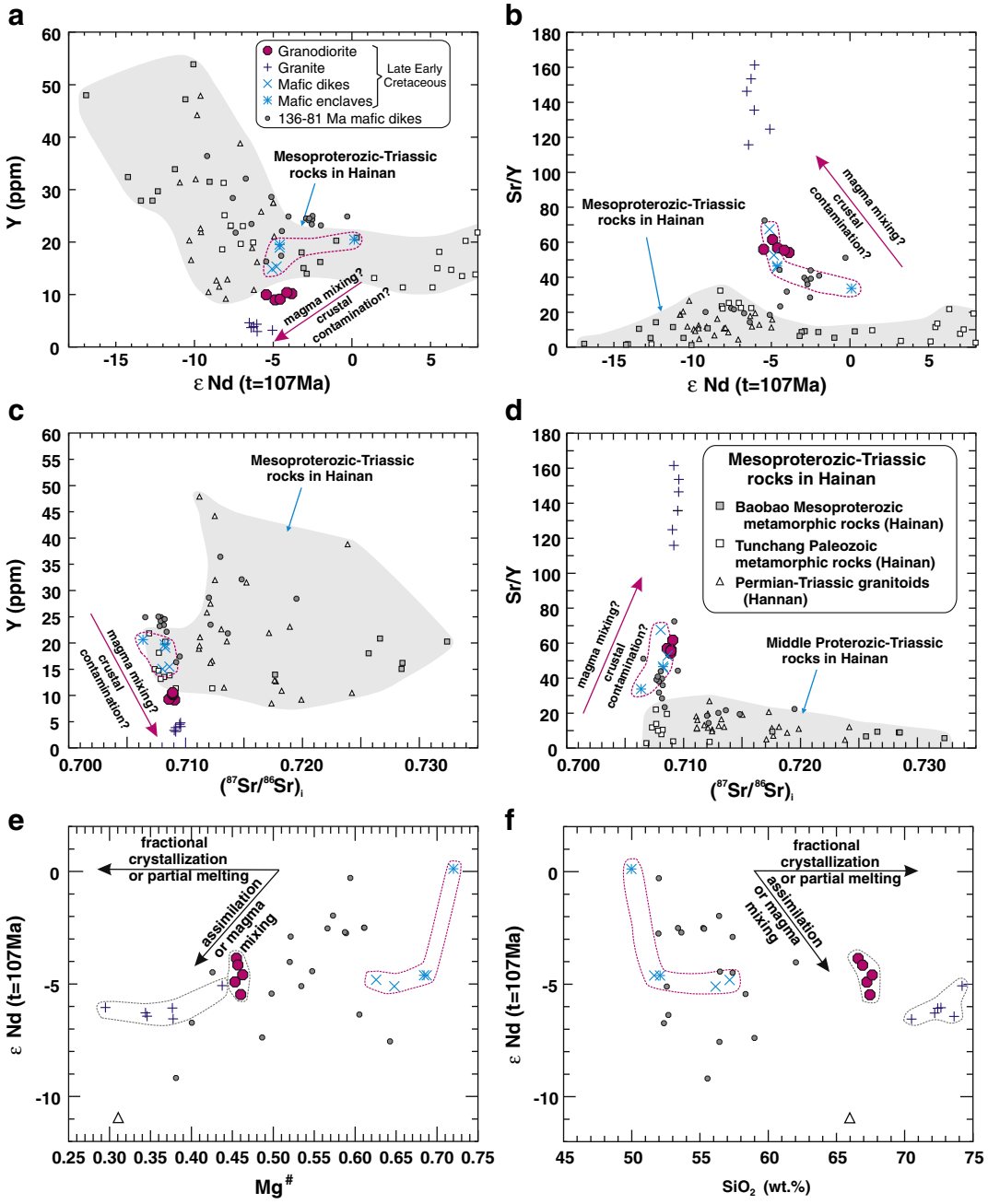

Fig. 15. (a)εNd(t = 107 Ma) versus Y; (b)εNd(t = 107 Ma) versus Sr/Y; (c) $(^{87}Sr/^{86}Sr)_i$ versus Y; (d) $(^{87}Sr/^{86}Sr)_i$ versus Sr/Y; (e) $Mg^{\#}$ versusεNd(t = 107 Ma); (f) SiO_2 versusεNd(t = 107 Ma). The data for Mesoproterozoic–Triassic metamorphic and magmatic rocks and 136–81 ma mafic dikes in the Hainan Island are from Xu et al. (2000, 2007, 2008), Ge (2003), Ge et al. (2003), Yun et al. (2005), Li et al. (2006a), Li et al. (2008), and references therein.

metabasaltic and eclogite melts at high pressures of 1.0–4.0 GPa (Fig. 11b), or adakitic rocks derived from thickened lower crust (e.g., Atherton and Petford, 1993; Wang et al., 2005a, 2007c).

The typically arc-like trace element patterns (Fig. 10b), the negative εNd(t) (−3.9 to −6.5) and the relatively old Nd model ages (1.31–1.06 Ga) (Appendix 6) of the Tungchang–Fengmu adakitic rocks all suggest that they originated from old (Neoproterozoic or Mesoproterozoic) arc-type crustal rocks (Zhou et al., 2002, 2006b; Wu et al., 2006b; Zheng et al., 2008). The Hainan region is part of Cathaysia Block, which contains well-documented Mesoproterozoic (~1400 Ma) metavolcanic–intrusive–sedimentary rocks (Fig. 1b) (e.g., Li et al., 2008) but lacks any known record of Neoproterozoic metamorphic rocks. The Nd–Sr isotopic compositions of the Tungchang–Fengmu adakitic rocks, however, differ from those of any Proterozoic–Triassic rocks on Hainan Island, including the Mesoproterozoic rocks (Fig. 12a). The εHf(t) values of their ~107 Ma zircons are also distinctly higher than those of 212–819 Ma xenocrystic zircons in Late Permian–late Early Cretaceous intrusive rocks from Tunchang–Fengmu or the ~257 Ma zircons in the Late Permian Huogedun granodiorites (Fig. 12a–f). These observations suggest that the adakitic suite could not have been derived by partial melting of old crustal rocks despite their arc-like trace element characteristics and old Nd model ages.

On the other hand, the adakitic suite exhibits Nd–Sr isotopic compositions that are similar to those of Cretaceous mafic dikes on Hainan Island (Ge, 2003; Ge et al., 2003) (Fig. 12a–b), and the εHf(t) values of their respective ~107 Ma and 119–168 Ma zircons are also similar (Fig. 13a–c, g–h). Such similarities are consistent with the adakitic suite being sourced from Jurassic–Early Cretaceous (168–119 Ma) underplated mafic rocks in the lower curst. For example, lower crustal mafic granulite xenoliths from Cenozoic basalts on the southeast China coast have Early Cretaceous crystallization ages (115–112 Ma), arc-like trace element characteristics and variable εNd(t) (−9.5 to +7.0) and $(^{87}Sr/^{86}Sr)_i$ (7030–0.7107) (Fig. 12a), which indicates that they were derived by the underplating of continental arc-type basaltic magmas near the crust–mantle boundary (Xu et al., 1996, 1999b; Yu et al., 2003). Notably, these mafic granulite xenoliths include examples with Nd–Sr isotope compositions that are similar to the Hainan Island Cretaceous mafic rocks and the Tungchang–Fengmu adakitic suite (Fig. 12a–b). Thus, we suggest that the adakitic rocks were most likely generated by partial melting of this newly underplated basaltic lower crust.

As noted above, the Niubiling and Gaotongling adakitic granites exhibit more depleted middle REE and HREE (Gd–Lu) patterns than the Tunchang adakitic granodiorites (Fig. 10a–b), suggesting that their source contained residual amphibole in addition to garnet (Gromet and Silver, 1987). Therefore, the Tunchang adakitic granodiorites were most plausibly produced by partial melting of basaltic lower crust in the garnet stability field whereas the Niubiling and Gaotongling adakitic granites were likely derived by partial melting of basaltic lower crust in the stability field of garnet + amphibole.

The high K_2O contents and K_2O/Na_2O ratios of the Tunchang–Fengmu suite differ from those of adakites derived from subducted oceanic crust (e.g., Defant and Drummond, 1990) but are similar to potassium-rich adakitic rocks generated in the lower crust (see detailed discussion in Wang et al. (2007c)). In such occurrences, the high K_2O contents are mainly attributed to high-pressure (1.0–4.0 GPa) and dehydration melting of high K_2O basaltic source

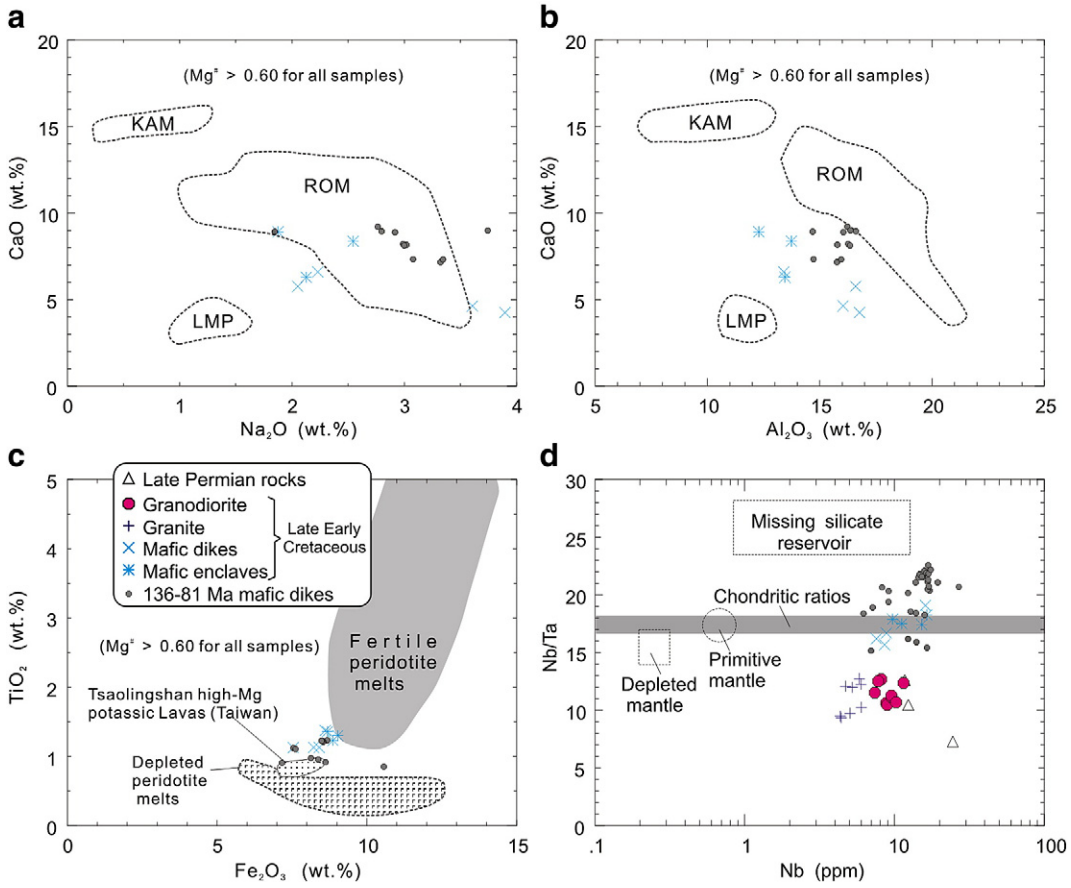

Fig. 16. (a–c) Petrological variations of mafic ($Mg^{\#} > 0.60$) potassic rocks; (d) Nb versus Nb/Ta. The fields for Cenozoic KAM-, LAM- and ROM-type mafic ($Mg^{\#} > 0.60$) potassic rocks in Italy are after Peccerillo (1999). The fields for fertile and depleted peridotite melts and subducted fluid-metasomatized harzburgitic source (lithospheric mantle)-derived Tsaolingshan high-Mg potassic Lavas in Taiwan are after Chung et al. (2001) and references therein. The field for primitive and depleted mantles, chondrite and missing silicate reservoir are from Barth et al. (2000) and references therein. The data for Cretaceous (136–81 Ma) mafic dikes in the central Hainan Island are from Ge (2003) and Ge et al. (2003).

rocks (Wang et al., 2007c). We suggest that similar factors were responsible for the high K_2O contents of the Tunchang–Fengmu adakitic rocks. First, their source (i.e., newly underplated basaltic lower crust) is likely to have been potassium-rich, given that Cretaceous mafic dikes in central Hainan Island have Nd–Sr isotope compositions similar to the adakitic rocks (Fig. 12a–b), and are shoshonitic or high-K calc-alkaline (Fig. 9b–c) (Ge, 2003; Ge et al., 2003). Second, the high K_2O contents and K_2O/Na_2O ratios of the adakitic rocks are similar to those of experimental melts generated by high-pressure (1–4.0 GPa) dehydration melting of metabasaltic and eclogite (Fig. 9a–c), rather than by low-pressure (<1.0 GPa) dehydration melting of metabasaltic rocks (Fig. 9a–c).

6.1.2. Evidence of magmatic mixing in magnesian- and K-rich mafic enclaves and dikes

Genetic models for mafic enclaves include origins as foreign xenoliths (usually country rocks) (e.g., Vernon, 1983; Bacon, 1986; Xu et al., 2006), refractory and residual phase assemblages derived from granitoid sources (e.g., Chappell et al., 1987; Chappell and White, 1991), chilled material or accumulations of early-formed co-genetic crystals (e.g., Tindle and Pearce, 1983; Bonin, 1991; Schonenberger et al., 2006; Shellnutt et al., 2010), and the products of mixing between distinct mafic and felsic magmas (e.g., Holden et al., 1987; Wiebe et al., 1997; Barbarin, 2005; Browne et al., 2006; Yang et al., 2006, 2007; Chen et al., 2009; Kent et al., 2010; Sun et al., 2010). The mafic enclaves in the Tunchang granodiorites are ellipsoidal, spindle-shaped, or elongate, and exhibit typical magmatic texture (Figs. 3e–g and 5a, c, e–g). Moreover, they are clearly different from the host country rocks (the Late Permian gneissic granodiorites) in terms of structure, texture (Fig. 3a, e–g), mineral compositions (Fig. 4) and geochemical composition (Fig. 9), and are therefore not xenoliths. In addition, if garnet was the main residual mineral in the source of the Tunchang adakitic granodiorites as suggested above, then these garnet-free mafic enclaves do not correspond to the refractory and residual phase assemblage of the adakitic granodiorite sources. Finally, the compositional gap between the mafic enclaves and Tunchang adakitic granodiorites (Fig. 9) indicates that the latter could not have been derived by fractional crystallization of mafic magmas, and the mafic enclaves cannot represent chilled material or accumulations of early formed genetically related crystals. Therefore, it is unlikely that any of the first three models explain the petrogenesis of the Tunchang mafic enclaves, although the mafic magmas might have undergone minor fractional crystallization of plagioclase (Fig. 14a–b).

We suggest that the mafic enclaves in the Tunchang granodiorites reflect hybridization between mantle-derived mafic and crust-derived felsic magmas based on the following evidence. Apart from one sample with the highest MgO contents and distinct Nd–Sr–Pb isotope compositions, the mafic enclaves are geochemically similar to mafic dikes in the Tunchang–Fengmu area and Cretaceous mafic dikes on central Hainan Island (Figs. 4 and 9–12), indicating that they likely have a similar petrogenesis. It is probable that mafic magmas were injected as dikes into the liquid interior of a felsic magma chamber where the magma was rapidly disaggregated and distributed by convection throughout the felsic magma (e.g., Pitcher, 1991; Wiebe et al., 1997; Chen et al., 2009). Some enclaves

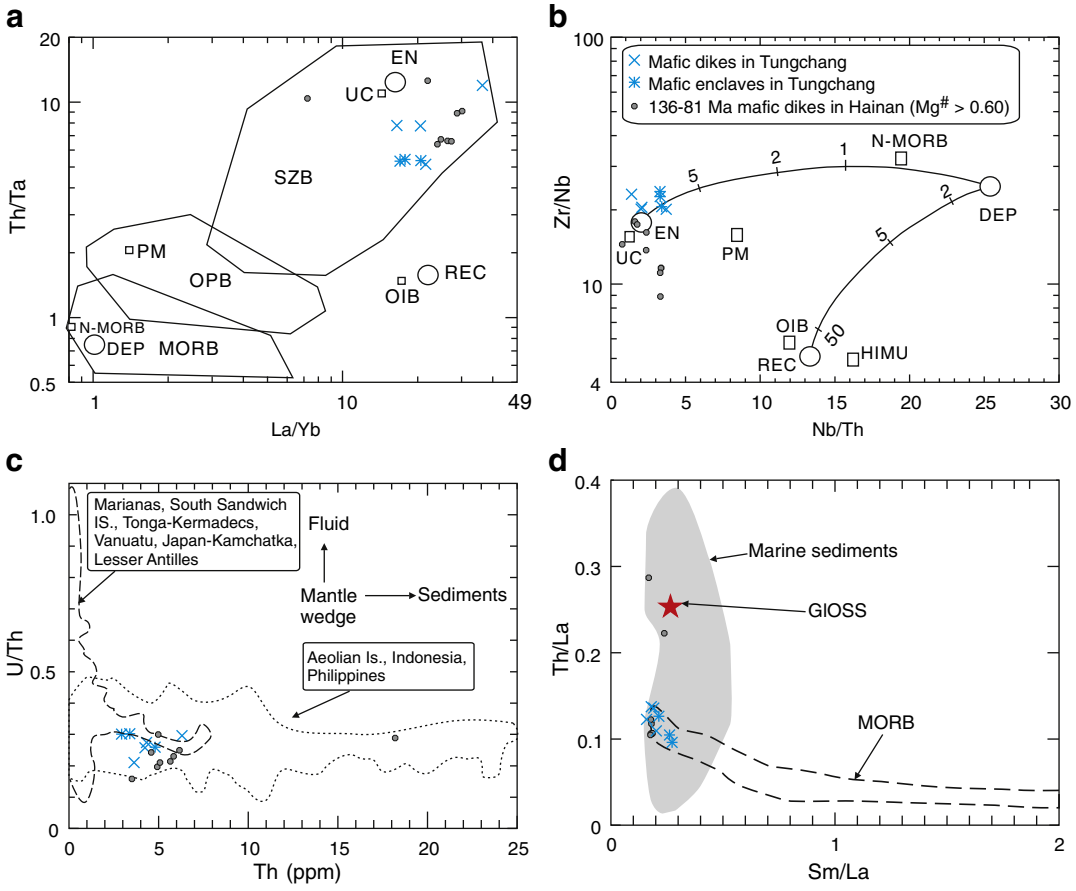

Fig. 17. (a–b) La/Yb versus Th/Ta and Nb/Th versus Zr/Nb diagrams for basalts (Condie et al., 2002). The fields for DEP (depleted mantle), EN (enriched mantle), MORB (middle oceanic ridge basalts), N-MORB (normal MORB), OIB (oceanic island basalts), OPB (oceanic plateau basalts), PM (primitive mantle), REC (recycled slab component), SZB (subduction zone basalts) and UC (upper continental crust) are after Condie et al. (2002) and references therein. (c) Th versus U/Th diagram (Hawkesworth et al., 1997). (d) Sm/La versus Th/La diagram (Plank, 2005). The field for MORB is after Plank (2005). The data for marine sediments and GLOSS (global subducted sediments) are from Plank and Langmuir (1998). The data for Cretaceous (136–81 Ma) mafic dikes in the central Hainan Island are from Ge (2003) and Ge et al. (2003).

would retain chemical and isotopic compositions similar to the injected magma (i.e., dikes), if they were large enough and rapidly quenched (Wiebe et al., 1997). This scenario suggests that the mafic enclaves and host rocks (the Tunchang granodiorites) represent two co-existing, compositionally distinct magmas (e.g., Chen et al., 2009). As noted above, however, disequilibrium features also occur in the mafic enclaves and dikes, including multiple zones (Fig. 5a–d) or distinctly low-MgO rims on high-MgO clinopyroxene phenocryst cores (Figs. 5e–f and 6), distinct compositional gaps in the Cr_2O_3 contents of clinopyroxene phenocryst cores and rims or matrix clinopyroxene grains (Fig. 6a), and close contact relationships between low-MgO rims of coarse clinopyroxene phenocrysts or small low-MgO matrix clinopyroxene grains and perthites + quartz or cryptocrystalline materials consisting of perthite (Pt) + quartz (Q) microcrystals (Fig. 5g, h). Moreover, feldspars of mafic enclaves and dikes in the Tungchang–Fengmu area consist of K-feldspar, albite and oligoclase (Fig. 4b), which is inconsistent with the low SiO_2 (48.33–54.63 wt.%) contents of their host rocks. Such a disequilibrium feature is inconsistent with simple crystallization processes. Rather, it indicates magma mixing (e.g., Troll and Schmincke, 2002). This raises the question of when and where the mixing occurred.

Evidence suggests that much of the mixing must have occurred prior to dike emplacement and enclave formation. (1) The mafic enclave sample with the highest MgO (11.34 wt.%) or $Mg^{\#}$ (0.72) values has the highest εNd(t) and lowest initial $^{87}Sr/^{86}Sr$, $^{207}Pb/^{208}Pb$ and $^{208}Pb/^{208}Pb$ ratios among all magmatic rocks in the Tunchang–Fengmu area, including the mafic dikes (Fig. 12), and may represent the most primitive magma composition in the area. However, this sample also contains disequilibrium features (Fig. 5a). Provided that the high-Mg mafic dikes (Appendix 5) correspond to the injected mafic magmas, but did not mix with the host felsic magmas (e.g., Wiebe et al., 1997; Chen et al., 2009), then the dikes and the most primitive enclaves must have undergone mixing before being injected. (2) As suggested above, the host granodiorite does not appear to have undergone extensive mixing with mafic magmas. (3) In order to calculate the parental melt compositions of the mafic enclaves and dikes, and the possible crustal end-member component involved in magma mixing, the melt compositions in equilibrium with clinopyroxene phenocryst cores (Cr > 2500 ppm) (early crystallization) and rims and matrix clinopyroxene grains (relatively late crystallization) are calculated in terms of their trace element contents using the method of Tiepolo and Tribuzio (2008) (Fig. 7c–d and Appendix 3). Except for some mobile large ion lithophile elements (e.g., Rb, B and Pb), most calculated element contents for melts equilibrated with clinopyroxene phenocryst cores are similar to those of mafic enclaves and dikes in the Tungchang–Fengmu area (Fig. 7c–d). However, the melts calculated to have been in equilibrium with clinopyroxene phenocryst rims and matrix clinopyroxene grains exhibit distinctly higher REE (LREE + HREE) contents than the adakitic intrusive rocks (Figs. 7c–d and 10), indicating that the adakitic magmas did not participate in magma mixing as a crustal end-member during dike emplacement and enclave formation. Therefore, it is possible that the mafic magmas injected into the adakitic magma chamber as dikes underwent mixing with felsic crustal melts at depth before being injected. In this case, the injected magma was broken up into discrete enclaves by convective motion of the adakitic magma (e.g., Chen et al., 2009) but rarely underwent further extensive mixing.

6.1.3. Mantle source of magnesian and K-rich mafic enclaves and dikes

The enclaves and dikes exhibit high-potassium characteristics, and some samples with high MgO and $Mg^{\#}$ values (Fig. 15e–f; Appendix 5) are actually similar to ultrapotassic rocks. However, their high-potassium characteristics could not have been generated by mixing of low K_2O basaltic magmas and relatively high K_2O crustal felsic magmas because the two enclave and dike samples with ultrapotassic characteristics have much higher K_2O contents than those of the Late Permian granodiorites and late Early Cretaceous adakitic rocks (Fig. 9b). As these ultrapotassic samples have high Cr (288–519 ppm) and $Mg^{\#}$ (0.66–0.72) values similar to primitive magmas (Tatsumi and Ishizaka, 1981), their compositions could not have been markedly modified by felsic crustal melts and the sample with the highest $Mg^{\#}$ (0.72) likely approximates the composition of the mantle-derived primitive magma. In fact, most trace element concentrations calculated for melts in equilibrium with clinopyroxene phenocryst cores are similar to those of the mafic enclaves and dikes in the Tungchang–Fengmu area (Fig. 7c–d), further supporting the above conclusions.

The magnesian ($Mg^{\#} = 0.63–0.72$) and potassium-rich mafic enclaves and dikes in the Tunchang–Fengmu area, as well as the Cretaceous mafic ($Mg^{\#} = 0.60–0.65$) dikes in central Hainan Island, exhibit relatively high Na_2O, CaO and Al_2O_3 contents, which are different from Cenozoic lamprotitic (LMP)- and kamafugitic (KAM)-type potassic mafic ($Mg^{\#} > 0.60$) lavas in Italy (Peccerillo, 1999) (Fig. 16a–b). Their compositional fields do, however, overlap those of Cenozoic Roman (ROM)-type potassic mafic lavas (Fig. 16a), or plot between those of the lamproitic (LMP)- and ROM-type potassic mafic lavas (Fig. 16b). The LMP-, KAM-, and ROM-type potassic mafic rocks are considered to have been derived from a restitic lithosperic mantle and fertile asthenospheric sources metasomatized by the introduction of a component similar to the deeply subducted upper crustal material, respectively (Peccerillo, 1999). In addition, on a Fe_2O_3 vs. TiO_2 diagram (Fig. 16c), the compositional field of the mafic enclaves and dikes are located between the fields of fertile and depleted peridotite melts. On a Nb vs. Nb/Ta diagram (Fig. 16d), they exhibit variable Nb/Ta ratios ranging from 15.2 to 22.6 (Appendix 5; Ge, 2003; Ge et al., 2003) similar to or slightly higher than those (15.5–17.4) of primitive mantle, chondrite or depleted mantle (Barth et al., 2000). Stolz et al. (1996) attributed the high Nb/Ta ratios (>17.0) of potassic mafic arc volcanics to modification of the subarc mantle source by silicic melts derived from the altered oceanic crust or subducted pelagic or terrigenous sediment, resulting in a phlogopite-bearing harzburgite/lherzolite or phlogopite orthopyroxenite/websterite. Therefore, these geochemical characteristics (Figs. 9a–c and 16) suggest that the Tunchang–Fengmu mafic and potassium-rich (high-K calc-alkaline and shoshonitic) enclaves and dikes contain components from both metasomatized asthenospheric and lithosperic mantle sources. They exhibit variable εNd(t) values (−5.1 to +0.1) that are clearly different from those of Middle Jurassic (~175–170 Ma) mafic rocks in central South China that were derived from an asthenospheric mantle source (Group 1) (Wang et al., 2008c), but are similar to those of Jurassic–Cretaceous (175–145 Ma) mafic rocks in the same area (Group 2) (Wang et al., 2008c). Their εNd(t) are also similar to those of Miocene NE Aegean shoshonites, which contain components from both enriched subcontinental lithospheric and asthenospheric mantle sources (Pe-Piper et al., 2009) (Fig. 12a–b), further supporting the above conclusions. In detail, the εNd(t) values of three of our mafic samples are essentially identical (enclave 07HN021 and dike samples 07HN012 and 016): εNd(t) = −4.6 to −4.8 over SiO_2 = 50.0 to 54.6 wt.% and Al_2O_3/TiO_2 between 10 and 15 (Appendices 5 and 6), which implies that these magmas acquired their isotopic signature in their subduction-modified source rather than through crustal AFC processes. Among all Late Permian–Cretaceous magmatic samples from the Tungchang–Fengmu area, enclave sample 07HN18 has the highest εNd(t) (+0.13) and $Mg^{\#}$ (0.72) and lowest SiO_2 (48.33 wt.%), and plots in the field of Pacific and N-Atlantic MORB on the Pb isotope composition diagram (Fig. 12c–d), suggesting that it did not undergo obvious crustal contamination and likely contains a higher proportion of metasomatized asthenospheric or relatively juvenile lithospheric mantle than other mafic rock samples.

Major elements (Na_2O, CaO and Al_2O_3) and Nb/Ta ratios (Fig. 16a–b and d) suggest that the mantle sources of the Tungchang–Fengmu mafic enclaves and dikes were metasomatized by silicic melts derived from subducted oceanic crust or sediments (Stolz et al., 1996; Peccerillo, 1999). The parental melts calculated to be in equilibrium with

clinopyroxene phenocryst cores exhibit clear Nb–Ta depletions similar to the Tungchang–Fengmu mafic enclaves and dikes (Fig. 7c–d), further indicating that their mantle source was modified by subducted fluid or sediments (Tatsumi, 1989; Hawkesworth et al., 1997). On La/Yb vs. Th/Ta and Nb/Th vs. Zr/Nb diagrams (Fig. 17a–b), these mafic enclave and dike samples plot in the field of subduction zone basalts (SZB) rather than oceanic plateau and mid-oceanic ridge basalts (OPB and MORB), and are close to the end member components of upper continental crust (UC) and enriched mantle (EN) rather than depleted mantle (DEP) or recycled slab (REC) (Condie et al., 2002). Their relatively low U/Th and Sm/La ratios and high Th and Th/La values (Fig. 17c–d; Ge, 2003; Ge et al., 2003) further suggest that their asthenospheric and lithosperic mantle source was metasomatized by subducted oceanic sediments (Hawkesworth et al., 1997; Plank, 2005).

6.2. Geodynamic processes

There are several different models for the evolution of South China during the Middle Permian–Triassic. For example, Li and Li (2007) proposed that subduction of Paleo-Pacific Oceanic Plate was initiated in the Mid-Permian and flat subduction of an oceanic plateau occurred between ca. 250 Ma and ca. 190 Ma. In this scenario, the 260–272 Ma Wuzhishan gneissic calc-alkaline I-type granites in central Hainan Island (Figs. 10 and 12; Li et al., 2006a; Zhang et al., 2011) were generated in a continental arc environment related to the initial subduction of the Paleo-Pacific oceanic plate beneath South China (Li et al., 2006a; Li and Li, 2007). However, Wang et al. (2007d) and Zhang et al. (2011) suggest that the Middle Permian–Triassic evolution of South China was related to the amalgamation of the Indochina and South China Blocks as the result of Paleotethys oceanic plate subduction and subsequent continental collision. Irrespective of these different viewpoints on the Middle Permian–Triassic evolution of South China, there has been a consensus that subduction of the Paleo-Pacific Plate and associated geodynamic processes (slab foundering or roll back or back-arc extension) played an important role in the Jurassic–Cretaceous evolution of the area (e.g., Xu et al., 1999a; Zhou and Li, 2000; Wang et al., 2005b; Zhou et al., 2006a; Li et al., 2006a; Li et al., 2007; Li and Li, 2007; Jiang et al., 2009, 2011; He et al., 2010; Zhao et al., 2012). These events can readily account for the combination of asthenospheric and lithosperic mantle wedge peridodite sources for the Tungchang–Fengmu intrusive suite and for their metasomatism by subducted oceanic sediments. The occurrence of 168–119 Ma magmatic zircons in these rocks, however, has important implications for Jurassic–Cretaceous geodynamic processes on Hainan Island.

Jurassic: Th ~107 Ma Tunchang–Fengmu intrusive rocks contain 168–160 Ma magmatic zircons, which are consistent with the widespread occurrence of 165–155 Ma I- and A-type granites and syenites following the initiation of intraplate basaltic and/or bimodal igneous magmatism at 190–170 Ma in central South China (e.g., Zhao et al., 1998, 2001; Chen et al., 2002; Li et al., 2003, 2004a, b, 2007; Wang et al., 2003, 2008c; He et al., 2010; Zhu et al., 2010) and Jurassic gabbros in the Hainan area (e.g., Liu, 1991). These Jurassic igneous rocks are considered to represent a major anorogenic magmatic event linked to foundering of an early Mesozoic subducted flat-slab beneath the SE China continent (Li and Li, 2007; Li et al., 2007) or lithospheric or back-arc extension induced by Jurassic subduction of the Paleo-Pacific Plate (e.g., Zhou et al., 2006a; He et al., 2010; Zhao et al., 2012). One 168–160 Ma inherited zircon crystal from the ~107 Ma intrusive suite exhibits positive εHf(f) values (Fig. 13g) that are different from those (<−2.0) of older zircons in ~257 Ma gneissic granodiorites and ~107 Ma intrusive rocks in the Tunchang–Fengmu area (Fig. 13e–f), indicating that underplating of mantle-derived magmas beneath the continental crust may have begun in the Jurassic (e.g., Zhou and Li, 2000).

Cretaceous: the ~107 Ma Tunchang–Fengmu suite contains 119–127 Ma magmatic zircons, which are consistent with the widespread presence of ~122–129 Ma A-type granites in the interior of South China (e.g., Wang et al., 2005b) and lithospheric extension that may have resulted from the roll-back of subducted Paleo-Pacific plate (e.g., Wong et al., 2009; Jiang et al., 2011). In this scenario, the resulting continuous upwelling of unmetasomatized asthenospheric mantle would have triggered partial melting of overlying subducted oceanic sediment-metasomatized asthenospheric and lithospheric mantle or relatively juvenile lithospheric mantle (e.g., Pe-Piper et al., 2009; Jiang et al., 2011) or interactions between melts derived from metasomatized asthenospheric mantle and lithospheric mantle (e.g., Chung et al., 1994; Xu et al., 2005). Basaltic magmas generated by these processes would have underplated, thickened and reworked the existing lower crust to form a new lower crust that itself was subject to melting as a result of continued basaltic magma underplating (Annen et al., 2006). Equilibration pressures and temperature calculations for 115–112 Ma lower crustal mafic granulite xenoliths in Cenozoic basalts from the southeast China coast show that they were generated at high temperatures (979–1224 °C) and pressures (0.85–1.6 GPa, corresponding to 28–53 km) (Xu et al., 1996, 1999b, Yu et al., 2003). This indicates that mafic magmatism and underplating in the lower crust may not only have caused the formation of a thickened lower crust, but also provided the thermal energy to produce approximately contemporaneous felsic magmatism in the region (e.g., Yu et al., 2003). Thus, partial melting of such a thickened new lower crust produced ~107 Ma adakitic magmas, which subsequently ascended to magma chambers at relatively shallow crustal depths. Synchronously, mantle-derived basaltic magmas, possibly mixed with minor felsic magmas of crustal origin, ascended and were injected into the adakitic magma chamber to form enclaves or dikes. We suggest that the proposed continuous upwelling of unmetasomatized asthenosphere as a result of subduction roll-back best accounts for the triggering of ~107 Ma crust- and mantle-derived magmatism and associated magma hybridization observed on Hainan Island.

7. Conclusions

In the Tunchang–Fengmu area, Hainan Island (South China), late Early Cretaceous (~107 Ma) granodiorites and biotite granites are associated with mafic enclaves and dikes. The granodiorites and biotite granites are geochemically similar to slab-derived adakites, e.g., high SiO_2, Al_2O_3, Sr, Sr/Y and La/Yb values, low Y and Yb contents, and negligible Eu and positive Sr anomalies. Major and trace element compositions, zircon ages and Nd–Sr–Pb–Hf isotope data suggest that they were most likely generated by partial melting of newly underplated basaltic lower crust. The mafic enclaves and dikes are high-K calc-alkaline and shoshonitic and most have high $Mg^{\#}$ (0.63–0.72) values. Petrographic textures and mineral compositions, along with geochemical and Nd–Sr–Pb–Hf isotope data for the most primitive examples, show that the magmas likely originated from asthenospheric + lithosperic mantle sources that had been metasomatized by subducted oceanic sediments, and subsequently underwent mixing with minor felsic magmas of crustal origin at depth. Late Early Cretaceous unmetasomatized asthenosphere upwelling due to the roll-back of subducted Paleo-Pacific plate may have triggered the crust- and mantle-derived magmatism and associated magma hybridization observed on the Hainan Island.

Acknowledgments

We sincerely thank Professors Y.F. Zheng, Klaus Mezger, and S.L. Chung and two anonymous reviewers for their constructive and helpful reviews and suggestions. We also appreciate the assistance of Jin-Hui Yang, Xi-Rong Liang, Xiang-Lin Tu, Lie-Wen Xie and Ying Liu for zircon age and geochemical analyses. Financial support for this research was provided by the Knowledge Innovation Program

of Chinese Academy of Sciences (KZCX1-YW-15-2) and the National Natural Science Foundation of China (nos. 41025006, 41073029 and 41121002). This is contribution no. IS-1506 from GIGCAS, TIGeR (The Institute for Geoscience Research) publication # 414, and contribution 173 from the ARC Centre of Excellence for Core to Crust Fluid Systems (http://www.ccfs.mq.edu.au/).

References

Andersen, T., 2002. Correction of common lead in U–Pb analyses that do not report ^{204}Pb. Chemical Geology 192, 59–79.
Annen, C., Blundy, J.D., Sparks, R.S.J., 2006. The genesis of intermediate and silicic magmas in deep crustal hot zones. Journal of Petrology 47 (3), 505–539.
Atherton, M.P., Petford, N., 1993. Generation of sodium-rich magmas from newly underplated basaltic crust. Nature 362 (6416), 144–146.
Bacon, C.R., 1986. Magmatic inclusions in silicic and intermediate rocks. Journal of Geophysical Research 81, 6091–6112.
Barbarin, B., 2005. Mafic magmatic enclaves and mafic rocks associated with some granitoids of the central Sierra Nevada batholith, California: nature, origin, and relations with the hosts. Lithos 80 (1–4), 155–177.
Barth, M.G., William, F., McDonough, W.F., Rudnick, R.L., 2000. Tracking the budget of Nb and Ta in the continental crust. Chemical Geology 165, 197–213.
Beard, J.M., Lofgren, G.E., 1991. Dehydration melting and water-saturated melting of basaltic and andesitic greenstones and amphibolites at 1.3, and 6.9 kb. Journal of Petrology 32, 365–401.
Belousova, E.A., Griffin, W.L., Suzanne, Y.O.R., Fisher, N.I., 2002. Igneous zircon: trace element composition as an indicator of source rock type. Contributions to Mineralogy and Petrology 143 (5), 602–622.
Bonin, B., 1991. The enclaves of alkaline anorogenic granites: an overview. In: Didier, J., Barbarin, B. (Eds.), Enclaves and Granite Petrology. : Developments in Petrology, 13. Elsevier, Amsterdam, pp. 179–189.
Bonin, B., 2004. Do coeval mafic and felsic magmas in post-collisional to within-plate regimes necessarily imply two contrasting, mantle and crustal, sources? A review. Lithos 78 (1–2), 1–24.
Browne, B.L., Eichelberger, J.C., Patino, L.C., Vogel, T.A., Dehn, J., Uto, K., Hoshizumi, H., 2006. Generation of porphyritic and equigranular mafic enclaves during magma recharge events at Unzen volcano, Japan. Journal of Petrology 47 (2), 301–328.
Castillo, P.R., Janney, P.E., Solidum, R.U., 1999. Petrology and geochemistry of Camiguin island, southern Philippines: Insights to the source of adakites and other lavas in a complex arc setting. Contributions to Mineralogy and Petrology 134, 33–51.
Chappell, B.W., White, A.J.R., 1991. Restite enclaves and the restite model. In: Didier, J., Barbarin, B. (Eds.), Developments in Petrology, 13. Elsevier, Amsterdam, pp. 375–381.
Chappell, B.W., White, A.J.R., Wyborn, D., 1987. The importance of residual source material (restite) in granite petrogenesis. Journal of Petrology 28, 1111–1138.
Chen, J.F., Jahn, B.M., 1998. Crustal evolution of Southeastern China: Nd and Sr isotopic evidence. Tectonophysics 284, 101–133.
Chen, P.R., Hua, R.M., Zhang, B.T., Lu, J.J., Fan, C.F., 2002. Early Yanshanian post-orogenic granitoids in the Nanling region: petrological constraints and geodynamic settings. Science in China, Series D 45 (8), 755–768.
Chen, B., Chen, Z.C., Jahn, B.M., 2009. Origin of mafic enclaves from the Taihang Mesozoic orogen, North China craton. Lithos 110 (1–4), 343–358.
Chen, C.-H., Hsieh, P.-S., Lee, C.-Y., Zhou, H.-W., 2011. Two episodes of the Indosinian thermal event on the South China block: constraints from LA-ICPMS U–Pb zircon and electron microprobe monazite ages of the Darongshan S-type granitic suite. Gondwana Research 19 (4), 1008–1023.
Chung, S.L., Sun, S.S., Tu, K., 1994. Late Cenozoic basaltic volcanism around the Taiwan Strait, SE China: product of lithosphere–asthenosphere interaction during continental extension. Chemical Geology 112, 1–20.
Chung, S.-L., Wang, K.-L., Crawford, A.J., Kamenetsky, V.S., Chen, C.-H., Lan, C.-Y., Chen, C.-H., 2001. High-Mg potassic rocks from Taiwan: implications for the genesis of orogenic potassic lavas. Lithos 59 (4), 153–170.
Chung, S.-L., Liu, D., Ji, J., Chu, M.-F., Lee, H.-Y., Wen, D.-J., Lo, C.-H., Lee, T.-Y., Qian, Q., Zhang, Q., 2003. Adakites from continental collision zones: melting of thickened lower crust beneath southern Tibet. Geology 31 (11), 1021–1024.
Condie, K.C., Frey, B.A., Kerrich, R., 2002. The 1.75 Ga Iron King Volcanics in west-central Arizona: a remnant of an accreted oceanic plateau derived from a mantle plume with a deep depleted component. Lithos 64, 49–62.
Defant, M.J., Drummond, M.S., 1990. Derivation of some modern arc magmas by melting of young subducted lithosphere. Nature 347, 662–665.
Defant, M.J., Xu, J.F., Kepezhinskas, P., Wang, Q., Zhang, Q., Xiao, L., 2002. Adakites: some variations on a theme. Acta Petrologica Sinica 18 (2), 129–142.
Didier, J., 1973. Granites and their enclaves; the bearing of enclaves on the origin of granites. The Bearing of Enclaves on the Origin of Granites, Development in Petrology, vol. 3. Elsevier, Amsterdam.
Didier, J., Barbarin, B., 1991. Enclaves and granite petrology. Developments in Petrology, vol. 13. Elsevier, Amsterdam. 625 pp.
Drummond, M.S., Defant, M.J., Kepezhinskas, P.K., 1996. The petrogenesis of slab derived trondhjemite–tonalite–dacite/adakite magmas. Transactions of the Royal Society of Edinburgh Earth Science 87, 205–216.
Eberz, G.W., Nicholls, I.A., Maas, R., McCulloch, M.T., Whitford, D.J., 1990. The Nd- and Sr-isotopic composition of I-type microgranitoid enclaves and their host rocks from the Swifts Creek Pluton, southeast Australia. Chemical Geology 85 (1–2), 119–134.
Foley, S.F., Venturelli, G., Green, D.H., Toscani, L., 1987. The ultrapotassic rocks: characteristics, classification, and constraints for petrogenetic models. Earth-Science Reviews 24 (2), 81–134.
Gao, S., Rudnick, R.L., Yuan, H.L., Liu, X.M., Liu, Y.S., Xu, W.L., Ling, W.L., Ayers, J., Wang, X.C., Wang, Q.H., 2004. Recycling lower continental crust in the North China craton. Nature 432 (7019), 892–897.
Ge, X. Y., 2003. Mesozoic Magmatism in Hainan Island (SE China) and its tectonic significance: geochronology, geochemistry and Sr–Nd isotope evidence. Ph. D. thesis, Chinese Academy of Sciences, Beijing, China (in Chinese with English abstract). P. 1–87.
Ge, X.Y., Li, X.H., Zhou, H.W., 2003. Geochronologic, geochemistry and Sr–Nd istopes of the Late Cretaceous mafic dike swarms in southern Hainan Island. Geochimica 32 (1), 11–20 (in Chinese with English abstract).
Gromet, L.P., Silver, L., 1987. REE variations across the peninsular ranges batholith: implications for batholithic petrogenesis and crustal growth in magmatic arcs. Journal of Petrology 28, 75–125.
Guo, F., Nakamuru, E., Fan, W.M., Kobayoshi, K., Li, C.W., 2007. Generation of Palaeocene adakitic andesites by magma mixing in Yanji Area, NE China. Journal of Petrology 48 (4), 661–692.
Hawkesworth, C.J., Turner, S.P., Mcdermott, F., Peate, D.W., van Calsteren, P., 1997. U–Th isotopes in arc magmas: implications for element transfer from subducted crust. Science 276, 551–555.
He, Z.-Y., Xu, X.-S., Niu, Y., 2010. Petrogenesis and tectonic significance of a Mesozoic granite–syenite–gabbro association from inland South China. Lithos 119 (3–4), 621–641.
Holden, P., Halliday, A.N., Stephens, W.E., 1987. Neodymium and strontium isotope content of microdiorite enclaves points to mantle input to granitoid production. Nature 330 (6143), 53–56.
Huang, X.L., Xu, Y.G., Lo, C.H., Wang, R.C., Lin, C.Y., 2007. Exsolution lamellae in a clinopyroxene megacryst aggregate from Cenozoic basalt, Leizhou Peninsula, South China: petrography and chemical evolution. Contributions to Mineralogy and Petrology 154, 691–705.
Huang, F., Li, S., Dong, F., He, Y., Chen, F., 2008. High-Mg adakitic rocks in the Dabie orogen, central China: implications for foundering mechanism of lower continental crust. Chemical Geology 255 (1–2), 1–13.
Jia, X.H., Wang, Q., Tang, G.J., Jiang, Z.Q., Zhao, Z.H., Yang, Y.H., Wang, X.D., Zhao, W.Q., 2010. Zircon U–Pb geochronology, geochemistry and petrogenesis of the Late Early Cretaceous adakitic intrusive rocks in the Tunchang area, Hainan Province. Geochemica 39 (6), 497–519 (in Chinese with English abstract).
Jiang, Y.-H., Jiang, S.-Y., Dai, B.-Z., Liao, S.-Y., Zhao, K.-D., Ling, H.-F., 2009. Middle to late Jurassic felsic and mafic magmatism in southern Hunan province, southeast China: implications for a continental arc to rifting. Lithos 107 (3–4), 185–204.
Jiang, Y.-H., Zhao, P., Zhou, Q., Liao, S.-Y., Jin, G.-D., 2011. Petrogenesis and tectonic implications of Early Cretaceous S- and A-type granites in the northwest of the Gan-Hang rift, SE China. Lithos 121 (1–4), 55–73.
Kay, R.W., Kay, S.M., 1993. Delamination and delamination magmatism. Tectonophysics 219 (1–3), 177–189.
Kay, S.M., Ramos, V.A., Marquez, M., 1993. Evidence in Cerro Pampa volcanic rocks for slab-melting prior to ridge-trench collision in southern South America. Journal of Geology 101, 703–714.
Kent, A.J.R., Darr, C., Koleszar, A.M., Salisbury, M.J., Cooper, K.M., 2010. Preferential eruption of andesitic magmas through recharge filtering. Nature Geoscience 3 (9), 631–636.
Koyaguchi, T., Kaneko, K., 1999. A two-stage thermal evolution model of magmas in continental crust. Journal of Petrology 40 (2), 241–254.
Leake, B.E., et al., 1997. Nomenclature of amphiboles; report of the subcommittee on amphiboles of the International Mineralogical Association, Commission on New Minerals and Mineral Names. American Mineralogist 82 (9–10), 1019–1037.
Li, X.H., 2000. Cretaceous magmatism and lithospheric extension in Southeast China. Journal of Asian Earth Sciences 18 (3), 293–305.
Li, Z.X., Li, X.H., 2007. Formation of the 1300-km-wide intracontinental orogen and postorogenic magmatic province in Mesozoic South China: a flat-slab subduction model. Geology 35 (2), 179–182.
Li, X.H., Zhou, H., Chung, S.L., Ding, S., Liu, Y., Lee, C.Y., Ge, W., Zhang, Y., Zhang, R., 2002a. Geochemical and Sm–Nd isotopic characteristics of metabasites from central Hainan Island, South China and their tectonic significance. Island Arc 11, 193–205.
Li, Z.-X., Li, X.-h., Zhou, H., Kinny, P.D., 2002b. Grenvillian continental collision in south China: new SHRIMP U–Pb zircon results and implications for the configuration of Rodinia. Geology 30 (2), 163–166.
Li, X.H., Chen, Z.G., Liu, D.Y., Li, W.X., 2003. Jurassic gabbro–granite–syenite suites from southern Jiangxi Province, SE China: age, origin and tectonic significance. International Geology Review 45, 898–921.
Li, X.H., Liu, D.Y., Sun, M., Li, W.X., Liang, X.R., Liu, Y., 2004a. Precise Sm–Nd and U–Pb isotopic dating of the super-giant Shizhuyuan polymetallic deposit and its host granite, southeast China. Geological Magazine 141, 225–231.
Li, X.H., Chung, S.L., Zhou, H.W., Lo, C.H., Liu, Y., Chen, C.H., 2004b. Jurassic intraplate magmatism in southern Hunan-eastern Guangxi: ^{40}Ar/^{39}Ar dating, geochemistry, Sr–Nd isotopes and implications for tectonic evolution of SE China. In: Malpas, J., Fletcher, C.J., Aitchison, J.C., Ali, J. (Eds.), Aspects of the Tectonic Evolution of China: Geological Society, London, Special Publications, 226, pp. 193–216.
Li, X.H., Li, Z.X., Li, W.X., Wang, Y.J., 2006a. Initiation of the Indosinian orogeny in South China: evidence for a Permian magmatic arc on the Hainan Island. Journal of Geology 114 (114), 341–353.
Li, X.H., Li, Z.X., Wingate, M.T.D., Chung, S.L., Liu, Y., Lin, G.C., Li, W.X., 2006b. Geochemistry of the 755 Ma Mundine Well dyke swarm, northwestern Australia:

part of a Neoproterozoic mantle superplume beneath Rodinia? Precambrian Research 146 (1–2), 1–15.
Li, X.H., Li, Z.X., Li, W.X., Liu, Y., Yuan, C., Wei, G.J., Qi, C.S., 2007. U–Pb zircon, geochemical and Sr–Nd–Hf isotopic constraints on age and origin of Jurassic I- and A-type granites from central Guangdong, SE China: a major igneous event in respond to foundering of a subducted flat-slab? Lithos 96, 186–204.
Li, Z.X., Li, X.H., Li, W.X., Ding, S.J., 2008. Was Cathaysia part of Proterozoic Laurentia? New data from Hainan Island, south China. Terra Nova 20, 154–164.
Li, J.-W., Zhao, X.-F., Zhou, M.-F., Ma, C.-Q., de Souza, Z., Vasconcelos, P., 2009. Late Mesozoic magmatism from the Daye region, eastern China: U–Pb ages, petrogenesis, and geodynamic implications. Contributions to Mineralogy and Petrology 157 (3), 383–409.
Ling, M.-X., Wang, F.-Y., Ding, X., Hu, Y.-H., Zhou, J.-B., Zartman, R.E., Yang, X.-Y., Sun, W., 2009. Cretaceous ridge subduction along the lower Yangtze River Belt, eastern China. Economic Geology 104 (2), 303–321.
Liu, G.M., 1991. New progress in research on granitic intrusives, Hainan Island. Guangdong Geology 6 (4), 87–94.
Liu, Y.S., Hu, Z.C., Gao, S., Güntherr, D., Xu, J., Gao, C.G., Chen, H.H., 2008. In situ analysis of major and trace elements of anhydrous minerals by LA-ICP-MS without applying an internal standard. Chemical Geology 257 (1–2), 34–43.
Liu, S.-A., Li, S., He, Y., Huang, F., 2010a. Geochemical contrasts between early Cretaceous ore-bearing and ore-barren high-Mg adakites in central-eastern China: implications for petrogenesis and Cu–Au mineralization. Geochimica et Cosmochimica Acta 74 (24), 7160–7178.
Liu, Y.S., Gao, S., Gao, C.G., Wang, D.B., Zong, K.Q., Hu, Z.C., 2010b. Timing of melt–peridotite interactions in xenoliths of the Trans-North China Orogen: U–Pb dating, Hf isotopes and trace elements in zircon. Journal of Petrology 51 (1–2), 537–571.
Macpherson, C.G., Dreher, S.T., Thirlwall, M.F., 2006. Adakites without slab melting: high pressure differentiation of island arc magma, Mindanao, the Philippines. Earth and Planetary Science Letters 243, 581–593.
Martin, H., Smithies, R.H., Rapp, R., Moyen, J.F., Champion, D., 2005. An overview of adakite, tonalite–trondhjemite–granodiorite TTG, and sanukitoid: relationships and some implications for crustal evolution. Lithos 79, 1–24.
Middlemost, E.A.K., 1994. Naming materials in the magma/igneous rock system. Earth-Science Reviews 37 (3–4), 215–224.
Morimoto, N., Fabries, J., Ferguson, A.K., Ginzburg, I.V., Ross, M., Seifert, F.A., Zussman, J., Aoki, K., Gottardi, G., 1988. Nomenclature of pyroxenes. American Mineralogist 73 (9–10), 1123–1133.
Nachit, H., Razafimahefa, N., Stussi, J.M., Carron, J.P., 1985. Biotite chemical compositions and magmatic typology of the granitoids. Comptes Rendus de l'Académie des Sciences 301, 813–818.
Peccerillo, A., 1999. Multiple mantle metasomatism in central-southern Italy: geochemical effects, timing and geodynamic implications. Geology 27, 315–318.
Peccerillo, A., Taylor, S.R., 1976. Geochemistry of Eocene calc-alkaline volcanic rocks from the Kastamonu area, Northern Turkey. Contributions to Mineralogy and Petrology 58 (1), 63–81.
Pe-Piper, G., Piper, D.J.W., Koukouvelas, I., Dolansky, L.M., Kokkalas, S., 2009. Postorogenic shoshonitic rocks and their origin by melting underplated basalts: the Miocene of Limnos, Greece. Geological Society of America Bulletin 121 (1–2), 39–54.
Petford, N., Atherton, M., 1996. Na-rich partial melts from newly underplated basaltic crust: the Cordillera Blanca Batholith, Peru. Journal of Petrology 37, 1491–1521.
Pitcher, W.S., 1991. Synplutonic dikes and mafic enclaves. In: Didier, J., Barbarin, B. (Eds.), Enclaves and Granite Petrology. Developments in Petrology, vol. 13. Elsevier, Amsterdam, pp. 383–391.
Plank, T., 2005. Constraints from thorium/lanthanum on sediment recycling at subduction zones and the evolution of the continents. Journal of Petrology 46 (5), 921–944.
Plank, T., Langmuir, C.H., 1998. The chemical composition of subducting sediment and its consequences for the crust and mantle. Chemical Geology 145, 325–394.
Rapp, R.P., Watson, E.B., 1995. Dehydration melting of metabasalt at 8–32 kbar: implications for continental growth and crust–mantle recycling. Journal of Petrology 36, 891–931.
Rapp, R.P., Shimizu, N., Norman, M.D., Applegate, G.S., 1999. Reaction between slab-derived melts and peridotite in the mantle wedge: experimental constraints at 3.8 GPa. Chemical Geology 160, 335–356.
Richards, J.P., Kerrich, R., 2007. Special paper: adakite-like rocks: their diverse origins and questionable role in metallogenesis. Economic Geology 102 (4), 537–576.
Robert, M.P., Clemene, J.D., 1993. Origin of high-potassium, calc-alkaline, I-type granidoids. Geology 21, 825–828.
Rudnick, R.L., 1995. Making continental crust. Nature 378 (6557), 571–578.
Schonenberger, J., Marks, M., Wagner, T., Markl, G., 2006. Fluid–rock interaction in autoliths of agpaitic nepheline syenites in the Ilimaussaq intrusion, South Greenland. Lithos 91, 331–351.
Sen, C., Dunn, T., 1994. Dehydration melting of a basaltic composition amphibolite at 1.5 and 2.0 GPa: implications for the origin of adakites. Contributions to Mineralogy and Petrology 117, 394–409.
Shellnutt, J.G., Jahn, B.M., Dostal, J., 2010. Elemental and Sr–Nd isotope geochemistry of microgranular enclaves from peralkaline A-type granitic plutons of the Emeishan large igneous province, SW China. Lithos 119 (1–2), 34–46.
Silva, M.M.V.G., Neiva, A.M.R., Whitehouse, M.J., 2000. Geochemistry of enclaves and host granites from the Nelas area, central Portugal. Lithos 50 (1–3), 153–170.
Skjerlie, K.P., Patiño Douce, A.E., 2002. The fluid-absent partial melting of a zoisite-bearing quartz eclogite from 1.0 to 3.2 GPa; implications for melting in thickened continental crust and for subduction-zone processes. Journal of Petrology 43, 291–314.
Springer, W., Seck, H.A., 1997. Partial fusion of basic granulites at 5 to 15 kbar: implications for the origin of TTG magmas. Contributions to Mineralogy and Petrology 127, 30–45.
Stern, C.R., Kilian, R., 1996. Role of the subducted slab, mantle wedge and continental crust in the generation of adakites from the Andean Austral Volcanic Zone. Contributions to Mineralogy and Petrology 123, 263–281.
Stolz, A.J., Jochum, K.P., Spettel, B., Hofmann, A.W., 1996. Fluid- and melt-related enrichment in the subarc mantle: evidence from Nb/Ta variations in island-arc basalts. Geology 24 (7), 587–590.
Streck, M.J., Leeman, W.P., Chesley, J., 2007. High-magnesian andesite from Mount Shasta: A product of magma mixing and contamination, not a primitive mantle melt. Geology 35, 351–354.
Sun, S.S., McDonough, W.F., 1989. Chemical and isotopic systematics of oceanic basalts: Implications for mantle composition and processes. In: Saunders, A.D., Norry, M.J. (Eds.), Implications for Mantle Composition and Processes, Magmatism in the Ocean Basins: Geological Society, London, Special publication, 42, pp. 313–345.
Sun, J.-F., Yang, J.-H., Wu, F.-Y., Li, X.-H., Yang, Y.-H., Xie, L.-W., Wilde, S.A., 2010. Magma mixing controlling the origin of the Early Cretaceous Fangshan granitic pluton, North China Craton: in situ U–Pb age and Sr-, Nd-, Hf- and O-isotope evidence. Lithos 120 (3–4), 421–438.
Sun, W., Zhang, H., Ling, M.-X., Ding, X., Chung, S.-L., Zhou, J., Yang, X.-Y., Fan, W., 2011. The genetic association of adakites and Cu–Au ore deposits. International Geology Review 53 (5), 691–703.
Tang, G.J., Wang, Q., Wyman, D.A., Li, Z.X., Zhao, Z.H., Jia, X.H., Jiang, Z.Q., 2010. Ridge subduction and crustal growth in the Central Asian Orogenic Belt: evidence from Late Carboniferous adakites and high-Mg diorites in the western Junggar region, northern Xinjiang (west China). Chemical Geology 277, 281–300.
Tatsumi, Y., 1989. Migration of fluid phases and genesis of basalt magmas in subduction zones. Journal of Geophysical Research 94, 4697–4707.
Tatsumi, Y., Ishizaka, K., 1981. Existence of andesitic primary magma: an example from southwest Japan. Earth and Planetary Science Letters 53, 124–130.
Tiepolo, M., Tribuzio, R., 2008. Petrology and U–Pb zircon geochronology of amphibole-rich cumulates with sanukitic affinity from Husky Ridge (Northern Victoria Land, Antarctica): insights into the role of amphibole in the petrogenesis of subduction-related magmas. Journal of Petrology 49 (5), 937–970.
Tindle, A.G., Pearce, J.A., 1983. Assimilation and partial melting of continental crust: evidence from the mineralogy and geochemistry of autoliths and xenoliths. Lithos 16, 185–202.
Troll, V.R., Schmincke, H.U., 2002. Magma mixing and crustal recycling recorded in ternary feldspar from compositionally zoned peralkaline Ignimbrite 'A', Gran Canaria, Canary Islands. Journal of Petrology 43 (2), 243–270.
Vernon, R.H., 1983. Restite, xenoliths and microgranitoid enclaves in granites. Journal and proceedings of the Royal Society of New South Wales 116, 77–103.
Vernon, R.H., 1984. Microgranitoid enclaves in granites; globules of hybrid magma quenched in a plutonic environment. Nature 309, 438–439.
Wang, X.F., Ma, D.Q., Jiang, D.H., 1991. Geology of Hainan Island (2): Igneous Rocks [M]. Geological Publishing House, Beijing, pp. 1–160 (in Chinese).
Wang, Y.J., Fan, W.M., Guo, F., Peng, T.P., 2003. Geochemistry of Mesozoic mafic rocks around the Chenzhou–Linwu fault in South China: implication for the lithospheric boundary between the Yangtze and the Cathaysia Blocks. International Geology Review 45 (3), 263–286.
Wang, Q., Xu, J.F., Zhao, Z.H., Bao, Z.W., Xu, W., Xiong, X.L., 2004a. Cretaceous high-potassium intrusive rocks in the Yueshan–Hongzhen area of east China: adakites in an extensional tectonic regime within a continent. Geochemical Journal 38 (5), 417–434.
Wang, Q., Zhao, Z.H., Bao, Z.W., Xu, J.F., Liu, W., Li, C.F., Bai, Z.H., Xiong, X.L., 2004b. Geochemistry and petrogenesis of the Tongshankou and Yinzu adakitic intrusive rocks and the associated porphyry copper–molybdenum mineralization in southeast Hubei, east China. Resource Geology 54 (2), 137–152.
Wang, Q., McDermott, F., Xu, J.F., Bellon, H., Zhu, Y.T., 2005a. Cenozoic K-rich adakitic volcanic rocks in the Hohxil area, northern Tibet: lower-crustal melting in an intracontinental setting. Geology 33, 465–468.
Wang, Q., Zhao, Z.H., Jian, P., Xiong, X.L., Bao, Z.W., Dai, T.M., Xu, J.F., Ma, J.L., 2005b. Geochronology of Cretaceous A-type granitoids or alkaline intrusive rocks in the hinterland, South China: constraints for Late-Mesozoic tectonic evolution. Acta Petrologica Sinica 21, 795–808.
Wang, Q., Xu, J.F., Jian, P., Bao, Z.W., Zhao, Z.H., Li, C.F., Xiong, X.L., Ma, J.L., 2006a. Petrogenesis of adakitic porphyries in an extensional tectonic setting, dexing, South China: implications for the genesis of porphyry copper mineralization. Journal of Petrology 47, 119–144.
Wang, Q., Wyman, D.A., Xu, J.F., Zhao, Z.H., Jian, P., Xiong, X.L., Bao, Z.W., Li, C.F., Bai, Z.H., 2006b. Petrogenesis of Cretaceous adakitic and shoshonitic igneous rocks in the Luzong area, Anhui Province (eastern China): implications for geodynamics and Cu–Au mineralization. Lithos 89 (3–4), 424–446.
Wang, Q., Wyman, D.A., Zhao, Z.H., Xu, J.F., Bai, Z.H., Xiong, X.L., Dai, T.M., Li, C.F., Chu, Z.Y., 2007a. Petrogenesis of Carboniferous adakites and Nb-enriched arc basalts in the Alataw area, northern Tianshan Range (western China): implications for Phanerozoic crustal growth in the Central Asia orogenic belt. Chemical Geology 236, 42–64.
Wang, Q., Wyman, D.A., Xu, J.F., Zhao, Z.H., Jian, P., Zi, F., 2007b. Partial melting of thickened or delaminated lower crust in the middle of eastern China: implications for Cu–Au mineralization. Journal of Geology 115 (2), 149–161.
Wang, Q., Wyman, D.A., Xu, J.F., Jian, P., Zhao, Z.H., Li, C., Xu, W., Ma, J.L., He, B., 2007c. Early Cretaceous adakitic granites in the Northern Dabie Complex, central China: implications for partial melting and delamination of thickened lower crust. Geochimica et Cosmochimica Acta 71, 2609–2636.

Wang, Y.J., Fan, W.M., Cawood, P.A., Ji, S.C., Peng, T.P., Chen, X.Y., 2007d. Indosinian high-strain deformation for the Yunkaidashan tectonic belt, South China: kinematics and $^{40}Ar/^{3}9Ar$ geochronological constraints. Tectonics 26, TC6008. http://dx.doi.org/10.1029/2007TC002099.

Wang, Q., Wyman, A., Xu, J.F., Wan, Y.S., Li, C.F., Zi, F., Jiang, Z.Q., Qiu, H.N., Chu, Z.Y., Zhao, Z.H., Dong, Y.H., 2008a. Triassic Nb-enriched basalts, magnesian andesites, and adakites of the Qiangtang terrane (Central Tibet): evidence for metasomatism by slab-derived melts in the mantle wedge. Contributions to Mineralogy and Petrology 155, 473–490.

Wang, Q., Wyman, D.A., Xu, J., Dong, Y., Vasconcelos, P.M., Pearson, N., Wan, Y., Dong, H., Li, C., Yu, Y., Zhu, T., Feng, X., Zhang, Q., Zi, F., Chu, Z., 2008b. Eocene melting of subducting continental crust and early uplifting of central Tibet: evidence from central-western Qiangtang high-K calc-alkaline andesites, dacites and rhyolites. Earth and Planetary Science Letters 272, 158–171.

Wang, Y.J., Fan, W.M., Cawood, P.A., Li, S.Z., 2008c. Sr–Nd–Pb isotopic constraints on multiple mantle domains for Mesozoic mafic rocks beneath the South China Block hinterland. Lithos 106, 297–308.

Wiebe, R.A., Smith, D., Sturm, M., King, E.M., Seckler, M.S., 1997. Enclaves in the Cadillac Mountain Granite (coastal Maine): samples of hybrid magma from the base of the chamber. Journal of Petrology 38 (3), 393–423.

Wong, J., Sun, M., Xing, G., Li, X.-h., Zhao, G., Wong, K., Yuan, C., Xia, X., Li, L., Wu, F., 2009. Geochemical and zircon U–Pb and Hf isotopic study of the Baijuhuajian metaluminous A-type granite: extension at 125–100 Ma and its tectonic significance for South China. Lithos 112 (3–4), 289–305.

Wu, F.Y., Yang, Y.H., Xie, L.W., Yang, J.H., Xu, P., 2006a. Hf isotopic compositions of the standard zircons and baddeleyites used in U–Pb geochronology. Chemical Geology 234 (1–2), 105–126.

Wu, R.X., Zheng, Y.F., Wu, Y.B., Zhao, Z.F., Zhang, S.B., Liu, X., Wu, F.Y., 2006b. Reworking of juvenile crust: element and isotope evidence from Neoproterozoic granodiorite in South China. Precambrian Research 146 (3–4), 179–212.

Xie, C.F., Zhu, J.C., Zhao, Z.J., Ding, S.J., Fu, T.A., Li, Z.H., Zhang, Y.M., Xu, D.M., 2005. Zircon SHRIM P U–Pb age dating of garnet–acmite syenite: constraints on the Hercynian–Indosinian tectonic evolution of Hainan Island. Geological Journal of China Universities 1l (1), 47–57.

Xie, C.F., Zhu, J.C., Ding, S.J., Zhang, Y.M., Fu, T.A., Li, Z.H., 2006. Identification of Hercynian shoshonitic intrusive rocks in central Hainan Island and its geotectonic implications. Chinese Science Bulletin 51 (20), 2507–2519.

Xie, G., Mao, J., Li, R., Bierlein, F.P., 2008. Geochemistry and Nd–Sr isotopic studies of Late Mesozoic granitoids in the southeastern Hubei Province, Middle-Lower Yangtze River belt, Eastern China: petrogenesis and tectonic setting. Lithos 104 (1–4), 216–230.

Xiong, X.L., Li, X.H., Xu, J.F., Li, W.X., Zhao, Z.H., Wang, Q., Chen, X.M., 2003. Extremely high-Na adakite-like magmas derived from alkali-rich basaltic underplate: the Late Cretaceous Zhantang andesites in the Huichang Basin, SE China. Geochemical Journal 37, 233–252.

Xu, X., O'Reilly, S.Y., Zhou, X., Griffin, W.L., 1996. A xenolith-derived geotherm and the crust–mantle boundary at Qilin, southeastern China. Lithos 38, 41–62.

Xu, X.S., Dong, C.W., Li, W.X., Zhou, X.M., 1999a. Late Mesozoic intrusive complexes in coastal area of Fujian, SE China: the significance of the gabbro–diorite–granite association. Lithos 46, 299–315.

Xu, X., Zhou, X., O'Reilly, S.Y., Tang, H., 1999b. Exploration for the lower crustal material and granite genesis in southeastern China. Acta Petrologica Sinica 15, 217–223 (in Chinese with English abstract).

Xu, D.R., Liang, X.Q., Tang, H.F., 2000. Geochemical characteristics of metamorphic basic volcanics from the Baoban Group, western Hainan and its tectonic implications. Geotectonica et Metallogenia 24 (4), 303–313 (in Chinese with English abstract).

Xu, J.F., Shinjo, R., Defant, M.J., Wang, Q., Rapp, R.P., 2002a. Origin of Mesozoic adakitic intrusive rocks in the Ningzhen area of east China: partial melting of delaminated lower continental crust? Geology 30 (12), 1111–1114.

Xu, J.F., Castillo, P.R., Li, X.H., Yu, X.Y., Zhang, B.R., Han, Y.W., 2002b. MORB-type rocks from the Paleo-Tethyan Mian-Lueyang northern ophiolite in the Qinling Mountains, central China: implications for the source of the low $^{206}Pb/^{204}Pb$ and high $^{143}Nd/^{144}Nd$ mantle component in the Indian Ocean. Earth and Planetary Science Letters 198, 323–337.

Xu, Y.-G., Ma, J.-L., Frey, F.A., Feigenson, M.D., Liu, J.-F., 2005. Role of lithosphere–asthenosphere interaction in the genesis of Quaternary alkali and tholeiitic basalts from Datong, western North China Craton. Chemical Geology 224, 247–271.

Xu, W., Gao, S., Wang, Q., Wang, D., Liu, Y., 2006. Mesozoic crustal thickening of the eastern North China craton: evidence from eclogite xenoliths and petrologic implications. Geology 34 (9), 721–724.

Xu, D.R., Xia, B., Li, P.-C., Chen, G.-H., Ma, C., Zhang, Y.-Q., 2007. Protolith natures and U–Pb sensitive high mass-resolution ion microprobe (SHRIMP) zircon ages of the metabasites in Hainan Island, South China: implications for geodynamic evolution since the late Precambrian. Island Arc 16 (4), 575–597.

Xu, D.R., Xia, B., Bakun-Czubarow, N., Bachlinski, R., Li, P., Chen, G., Chen, T., 2008. Geochemistry and Sr–Nd isotope systematics of metabasites in the Tunchang area, Hainan Island, South China: implications for petrogenesis and tectonic setting. Mineralogy and Petrology 92 (3), 361–391.

Yang, J.-H., Wu, F.-Y., Chung, S.-L., Wilde, S.A., Chu, M.-F., 2006. A hybrid origin for the Qianshan A-type granite, northeast China: geochemical and Sr–Nd–Hf isotopic evidence. Lithos 89 (1–2), 89–106.

Yang, J.-H., Wu, F.-Y., Wilde, S., Xie, L.-W., Yang, Y.-H., Liu, X.-M., 2007. Tracing magma mixing in granite genesis: in situ U–Pb dating and Hf-isotope analysis of zircons. Contributions to Mineralogy and Petrology 153 (2), 177–190.

Yu, J.-H., Xu, X., O'Reilly, S.Y., Griffin, W.L., Zhang, M., 2003. Granulite xenoliths from Cenozoic Basalts in SE China provide geochemical fingerprints to distinguish lower crust terranes from the North and South China tectonic blocks. Lithos 67 (1–2), 77–102.

Yun, P., Xie, S.Z., 2003. The genesis type of upper Mesozoic Tunchang rock body in Hainan Island and its tectonic significance. Guangdong Geology 18 (4), 9–14 (in Chinese with English abstract).

Yun, P., Lei, Y.H., Lü, C.Y., 2005. Sr and Nd isotopic constraints on the source regions of the Triassic granitiods in central-northern Hainan Island and their significance. Geotectonica et Metallogenia 29 (2), 234–241 (in Chinese with English abstract).

Zhang, C., Ma, C., Holtz, F., 2010. Origin of high-Mg adakitic magmatic enclaves from the Meichuan pluton, southern Dabie orogen (central China): implications for delamination of the lower continental crust and melt–mantle interaction. Lithos 119 (3–4), 467–484.

Zhang, F.F., Wang, Y.J., Chen, X.Y., Fan, W.M., Zhang, Y.H., Zhang, G.W., Zhang, A.M., 2011. Triassic high-strain shear zones in Hainan Island (South China) and their implications on the amalgamation of the Indochina and South China Blocks: kinematic and $^{40}Ar/^{39}Ar$ geochronological constraints. Gondwana Research 19 (4), 910–925.

Zhao, Z.H., Bao, Z.W., Zhang, B.Y., 1998. Geochemistry of the Mesozoic basaltic rocks in southern Hunan Province. Science in China, Series D 41, 102–113 (Supp.).

Zhao, Z.H., Bao, Z.W., Zhang, B.Y., Xiong, X.L., 2001. Crust–mantle interaction and its contribution to the Shizhuyuan superlarge tungsten polymetallic mineralization. Science in China, Series D 44 (3), 266–276.

Zhao, K.-D., Jiang, S.-Y., Yang, S.-Y., Dai, B.-Z., Lu, J.-J., 2012. Mineral chemistry, trace elements and Sr–Nd–Hf isotope geochemistry and petrogenesis of Cailing and Furong granites and mafic enclaves from the Qitianling batholith in the Shi-Hang zone, South China. Gondwana Research 22 (1), 310–324.

Zheng, Y.F., Wu, R.X., Wu, Y.B., Zhang, S.B., Yuan, H., Wu, F.Y., 2008. Rift melting of juvenile arc-derived crust: geochemical evidence from Neoproterozoic volcanic and granitic rocks in the Jiangnan Orogen, South China. Precambrian Research 163 (3–4), 351–383.

Zhou, X.M., Li, W.X., 2000. Origin of Late Mesozoic igneous rocks in Southeastern China: implications for lithosphere subduction and underplating of mafic magmas. Tectonophysics 326 (3–4), 269–287.

Zhou, M.F., Yan, D.P., Kennedy, A.K., Li, Y., Ding, J., 2002. SHRIMP U–Pb zircon geochronological and geochemical evidence for Neoproterozoic arc-magmatism along the western margin of the Yangtze Block, South China. Earth and Planetary Science Letters 196 (1–2), 51–67.

Zhou, M.-F., Yan, D.-P., Wang, C.-L., Qi, L., Kennedy, A., 2006a. Subduction-related origin of the 750 Ma Xuelongbao adakitic complex (Sichuan Province, China): implications for the tectonic setting of the giant Neoproterozoic magmatic event in South China. Earth and Planetary Science Letters 248 (1–2), 286–300.

Zhou, X.M., Sun, T., Shen, W.Z., Shu, L.S., Niu, Y.L., 2006b. Petrogenesis of Mesozoic granitoids and volcanic rocks in South China: a response to tectonic evolution. Episodes 29 (1), 26–33.

Zhu, B.Q., Chen, Y.W., Peng, J.H., 2001. Lead isotope geochemistry of the urban environment in the Pearl River Delta. Applied Geochemistry 16, 409–417.

Zhu, W.-G., Zhong, H., Li, X.-H., He, D.-F., Song, X.-Y., Ren, T., Chen, Z.-Q., Sun, H.-S., Liao, J.-Q., 2010. The early Jurassic mafic–ultramafic intrusion and A-type granite from northeastern Guangdong, SE China: age, origin, and tectonic significance. Lithos 119 (3–4), 313–329.